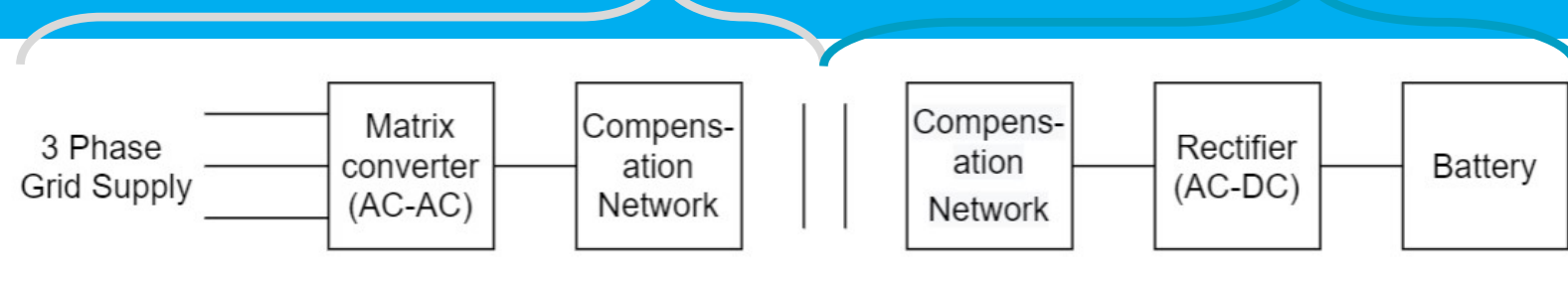
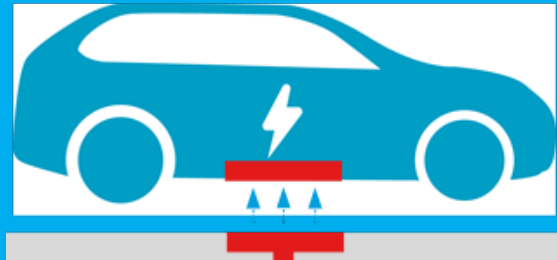


AC-AC Matrix Converter-based Grid-Side Power Converter for EV Wireless Charging

S. Mangudi Sankar



AC-AC Matrix Converter-based Grid-Side Power Converter for EV Wireless Charging

by

S. Mangudi Sankar

to obtain the degree of Master of Science
at the Delft University of Technology,

Student number: 5072883
Project duration: November 16, 2020 – August 2, 2021
Thesis committee: Dr. Thiago Batista Soeiro, TU Delft, supervisor
Dr. Jianning Dong, TU Delft
Dr. Aleksandra Lekic, TU Delft

This thesis is confidential and cannot be made public until August 2, 2021.

Abstract

The need for efficient power transfer at lower cost is a common requisite for any power converter system. When considering the application of wireless power transfer for Electric Vehicle (EV) charging, higher efficiency and lower cost can be achieved by reducing the number of stages of the system at the grid side. This thesis explores the feasibility of an AC/AC matrix converter for wireless power transfer application.

To begin with, different existing topologies of the converter module are discussed and qualitatively compared to the matrix converter. Subsequently, the plausibility of single stage matrix converter is verified through simulation. Due to the converter's high switching frequency, this configuration results in injection of higher than permitted harmonic content into the grid. Furthermore, the feasibility of three phase matrix converter and its advantages are studied. The converter working is verified through simulation.

To make the grid current less distorted, closed-loop control is introduced. This control consists of an inner current loop and an outer voltage loop which are both implemented using a PI controller.

To conclude, three phase matrix converter acts as a plausible solution for the desired application. Furthermore, the control ensures balanced grid current and desired output power.

Contents

1	Introduction	1
1.1	Motivation	1
1.2	Problem Statement	1
1.3	Research Questions.	2
1.4	Thesis Structure	2
2	Wireless Power Transfer System	5
2.1	Principles of wireless power transfer	5
2.2	Inductive power transfer (IPT)	6
2.3	IPT Systems for EV charging	6
2.3.1	Power supply architecture	7
2.3.2	Power electronics converters for the grid connection	7
2.3.3	Compensation Networks.	12
2.3.4	Mathematical analysis of the S-S compensation network.	13
2.3.5	Coupled Pads	14
2.3.6	Control of IPT systems	15
2.3.7	Standardization of IPT systems for EV charging	17
3	AC-AC Matrix Converters	19
3.1	Matrix Converter - Evolution, Circuit and its Working principle	19
3.2	Four-quadrant Switch	20
3.3	Commutation	21
3.4	Input filters	22
3.5	Matrix converters in WPT applications	22
4	Single Phase to Single Phase Matrix Converter	25
4.1	Implementation.	25
4.1.1	Four-quadrant switches-based model	25
4.1.2	Rectifier and H-bridge-based model	27
4.2	Single phase matrix converter for WPT in EV charging	30
4.3	Simulation of WPT model using DD coil	31
4.3.1	Analysis	32
4.3.2	Results	33
4.4	Zero Voltage Switching (ZVS)	34
4.4.1	Operating Principle	34
4.4.2	Resonant Tank Tuning	35
4.4.3	Bifurcation in WPT systems	35
4.4.4	Results	35
4.5	Input LC Filter	37
4.5.1	Damped LC Filter	39
4.6	Effect of input filter on inductor current	42
4.6.1	Ideal LC filter	42
4.6.2	Damped LC filter	42

5	Three Phase Matrix Converter	45
5.1	Implementation	45
5.2	Three-phase matrix converter for WPT application	46
5.2.1	DD coil based resonant tank	46
5.2.2	Rectangle coil based resonant tank	47
5.3	Evaluation of converter losses and system efficiency	50
5.3.1	Choice of the switching device	50
5.3.2	Semiconductor losses	52
5.4	Effect on load variation	54
5.5	Converter Control	54
5.5.1	Transfer function of converter with LC Filter	56
5.6	PI Current Controller	57
5.6.1	Results	58
6	Conclusion	61
6.1	Discussion	62
6.2	Future scope of work	62
A	Appendix	63
A.1	Fast Fourier Transform	63
A.2	Semiconductor Behaviour	68

Introduction

Power electronics has seen a rapid growth in the field of consumer and industrial electronics. The recent developments have led to the proliferation of Wireless Power Transfer (WPT) for Electric Vehicle (EV) charging. Wireless charging offers significant benefits over wired charging such as on-road charging, possible reduction in battery size and charging stations. It also eliminates risk factors such as the human interaction and entanglement of cables.

With the world moving towards sustainability, one of the most significant changes is the transition from fuel-powered cars to EVs. This transition gave rise to the development of charging infrastructure. The steep increase in usage of charging infrastructure necessitates research in alternative solutions to power the EVs.

In the current scenario, wired charging is the norm. This is realised in two forms : home/office with slow charging and commercial charging stations which offer fast charging. However, they require physical connection for the vehicle to be charged.

A plausible alternative solution is wireless transfer of power to charge the vehicle. This can be realised through inductive/capacitive coupling. Typically, WPT is implemented using a two-stage converter with distinct AC-DC and DC-AC conversion stages [1]. Another option could be the use of Matrix Converter, which carries out the AC-AC conversion in a single-stage [2].

1.1. Motivation

There is great space for development in the field of WPT, as mapped in Figure 1.1. The communication with reduced or no latency during data transfer is of prime importance for the control of WPT module. The power electronics and the passive modules constitute the overall loss in the system deteriorating the amount of power transferred and the system efficiency. The efficient design of power electronic modules and passive elements would eradicate the issues of misalignment to a certain extent, and it would as well boost the system efficiency. For any design of IPT systems, regulations and standards are of utmost importance. As suggested earlier, there is a vast range of open issues in the field of WPT which makes this research a popular topic.

1.2. Problem Statement

The objective of this thesis is to design an efficient AC-AC matrix converter for a 3.5 kW wireless charger for the application of EV. In specific, this research focuses on the feasibility of single-phase and three-phase matrix converters for the proposed application.

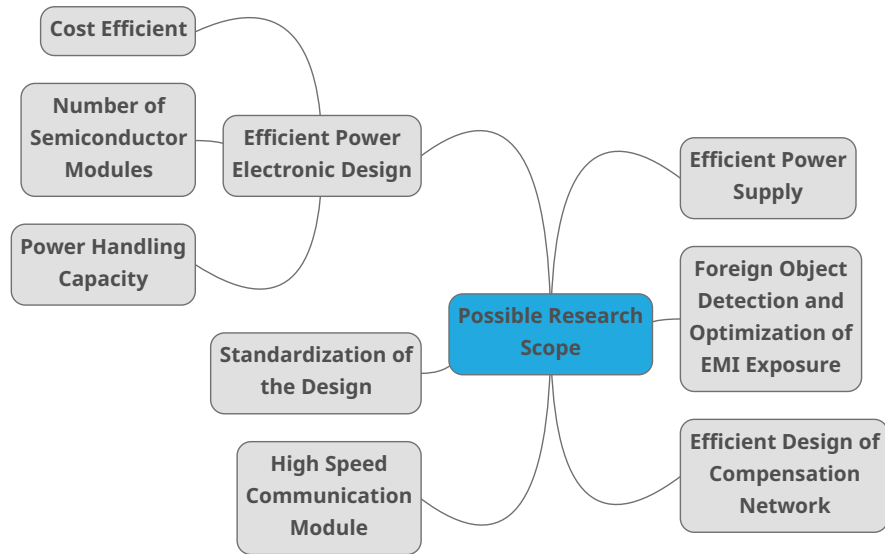


Figure 1.1: Feasible research scope in WPT-based charging system for EVs.

1.3. Research Questions

To verify the feasibility of the use of matrix converter in a WPT application for EV charging, the following research questions are set:

1. What are the possible configurations of power converters for the implementation of WPT in EV charging? What is the chosen configuration for this application?
2. How is the chosen configuration implemented for a single-phase grid connection?
3. Can the single-phase implementation be extended to a three-phase system? If yes, how?

1.4. Thesis Structure

The thesis is structured as follows:

- Chapter 1 introduces the concept of WPT for EV charging, the use of matrix converter for the application and defines the motivation, problem statement and the research questions for this thesis.
- Chapter 2 deals with the understanding of wireless power transfer mechanism and the detailed background on the complete module for EV applications. A comparison on different available power supply topologies is tabulated.
- Chapter 3 gives an introduction to matrix converter. It also explains different switching configurations, commutation and the need for input filters.
- Chapter 4 deals with the design of single phase matrix converter for the chosen WPT system. The feasibility of the designed converter is checked through simulations. The injection of harmonics into grid current due to the WPT system, is studied by comparing the results with the standards.

-
- Chapter 5 deals with the design of three phase matrix converter. The feasibility of the power electronic module is verified. The system efficiency, effect of bifurcation and its mitigation is studied. Finally, control of the converter is established to ensure balanced sinusoidal grid current and constant output power.

2

Wireless Power Transfer System

This chapter intends to be an overview of the wireless power transfer (WPT) technology focusing on the application of electric vehicles (EVs) charging. This chapter discusses primarily the physical principles of WPT. Inductive power transfer (IPT) with magnetic resonance for charging EVs is analysed with its main features such as compensation networks, power electronics, power supply, coupling pads, and control. After that, the commonly converters employed for the grid connection of EV wireless charging are summarized with a particular focus on AC-AC matrix converters.

2.1. Principles of wireless power transfer

WPT can be realized through three physical principles: microwave-based power transfer, Electric field-based power transfer and magnetic field-based power transfer.

- Microwave-based power transfer consists of radio field energy and it is transmitted via an antenna array which gets processed by a rectenna array or the receiver antenna. Primarily, the DC voltage input is converted to an RF signal which is fed to the transmitter antenna. The microwave beam is sent via the antenna to the rectenna. The rectenna is oriented to receive the output beam. The received beam is rectified back in the form of DC power such that it can be used by the power equipment. Generally, microwave-based power transfer focuses on long-distance transmission [3]. Microwave-based power transfer poses lots of challenges. The orientation of the transmitting and the receiving end must be properly aligned to reduce the emission of stray radiations. The losses that occur during this power transfer are phenomenally high.
- Electric field-based power transfer utilizes the concept of two coupled metallic plates to form a capacitor for transferring power. It is often referred to as capacitive power transfer [3]. This type of model is more advantageous during misalignment as the field between the plates bends, making it tolerant to variations of the plates' position. It is lightweight and cost-effective but poses quite a lot of issues like high-frequency requirement during operation. As the capacitance made out of parallel plates is small, the amount of power that can be transferred is limited, and hence high operating frequency is required to transfer the power efficiently.
- Magnetic field-based power transfer, also called inductive power transfer (IPT), comprises of two mutually coupled coils separated by an air gap. The coupling coefficient is typically small due to the presence of a large air gap and, in the application of EV wireless charging, the magnetic coupling is not fixed since the receiver coil can assume different

position with respect to the transmitter coil. Due to the relatively low and variable coupling coefficient, ensuring an efficient and constant power transfer is challenging. High efficient power transfer is maintained by optimizing the coils' quality factor and the operating frequency. By using polyphase or multimodular systems, a wide range of power level can be achieved [3]. The coils' quality factor and operating frequency are the key parameters in determining the distance between the transfer coils and the efficiency of the transfer.

Considering the efficiency, cost and operating frequency, the magnetic field coupling is the most viable solution to transfer power wirelessly for EV wireless charging. Moreover, the minimum required operating frequency is in kHz range for a considerable air gap.

2.2. Inductive power transfer (IPT)

The physical principles under which IPT works are Ampere's Law and Faraday's Law.

- Ampere's Law: When an electric current flows through a conductor in free space, it generates a magnetic field which is proportional to the amount of current, the permeability of free space, and the number of turns of the conductor [4].
- Faraday's Law: When a time-varying magnetic flux is coupled to a conductor, it induces a voltage in the conductor whose value is proportional to the rate of change in magnetic flux and the number of turns in that conductor [4].

According to the two laws, the magnetic field generated by the flow of a high-frequency current through the primary coil follows Ampere's law. On the other hand, according to Faraday's law, the time-varying magnetic field induces a voltage to the secondary coil.

As seen from the aforementioned laws, the primary and secondary coils act as a loosely coupled transformer due to the presence of a large air gap between them. Thereby, only a small portion of primary generated magnetic flux gets linked to the secondary coils. This leads to high leakage and low magnetizing inductance, thereby introducing a large amount of reactive power into the system. An increase in reactive power causes a substantial increase in the electrical stress on the switching devices and it can cause a thermal issue for high-power transmission. A passive network is normally connected to each coil to prevent the circulation of reactive power from the source [3]. These passive networks are called compensation networks, and more details can be found in Section 2.3.3.

2.3. IPT Systems for EV charging

A typical IPT system for EV wireless charging comprises of power electronics converters at both the transmitting and the receiving side, compensation networks, and the magnetic coils, also called pads, with a definite air gap separation between them. As shown in Figure 2.1, the IPT system can be fed from 50 Hz AC-grid supply. As a result, the IPT system requires a rectification stage at the input from AC power to DC power, including the power factor correction stage. The resulting DC voltage source is connected to an inverter and it gets converted into a high-frequency AC voltage. To compensate for the reactive power of the magnetic coils, a compensation network comprising of passive elements is used before feeding the high-frequency AC power to the magnetic coils. Likewise, in the receiving side, the receiver coil connected to the compensation network receives the transferred AC power. The compensation network at both the transmitting and the receiving side is tuned to eliminate the leakage inductance of the circuits at the inverter's operating frequency. As a result, the power transfer efficiency is

maximized [3]. The resulting output voltage from the compensation network is rectified and controlled through an appropriate power electronics regulator to charge the load battery.

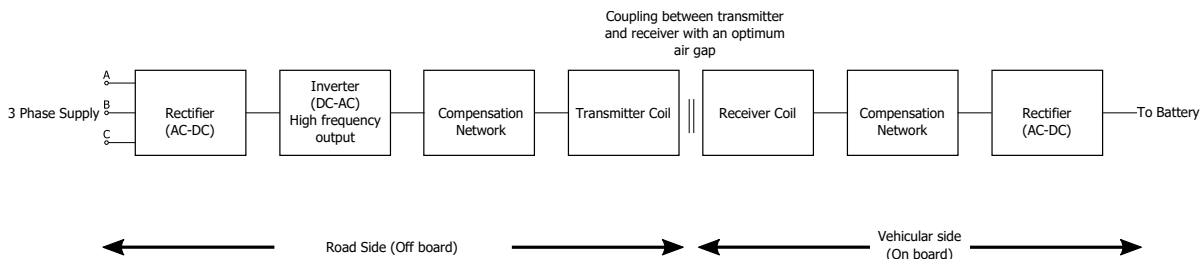


Figure 2.1: Traditional block schematic of a IPT system used in EV wireless charging.

2.3.1. Power supply architecture

Since the IPT system is generally powered by the (50 or 60) Hz grid, the grid-connection converter plays a vital role in accessing the IPT system. It also influences the IPT system's reliability and overall efficiency. The selection of a suitable power supply architecture is more challenging in the case of dynamic charging, also called in-motion charging [4], rather than in stationary charging which is motionless. In the case of motionless charging, at least one transmitter coil and one receiver coil are required to transmit power wirelessly and charge the EV's battery. But in the case of dynamic charging, the number of transmitter coils required depends on the design requirements. The traditional centralized supply structure shown in Figure 2.2(a) that powers all the transmitter pads can cause a potential decline in system reliability under severe conditions. Besides the centralized architecture, various power supply schemes can be implemented such as the segmented rail in Figure 2.2(b), and the high frequency segmented scheme in Figure 2.2(c).

The supply architectures used for the dynamic charging of electric vehicles are summarized in Table 2.1 [4]. The high frequency segmented power supply schemes and the segmented rail power supply schemes ensure relatively less power loss in the system. On the other hand, the segmented rail power supply scheme is less sensitive towards parameter change. Centralised power supply schemes possess a rectifier that converts the grid voltage to DC voltage which is then fed to the individual inverter and primary coil module. The system has high reliability due to the presence of individual inverter module for each of the transmitting pads. The system is cheap when compared to the segmented rail power supply as the latter needs litz wire between the inverter and the ground pad. In case copper wire is used, the AC resistance is high due to the presence of high frequency components and thus, the efficiency of the system is reduced.

2.3.2. Power electronics converters for the grid connection

Power electronics converters play a pivotal role in regulating the power flow through the WPT system. The converters at the input side control the AC power that feeds the IPT system. The converters at the output side rectify and regulate the received AC voltage for powering the battery.

At the input side, the desired power conversion can be realized with different PE converter structures that differ according to their number of stages. These structures can have a power conversion with either a single stage, two stages, or three-stages. In a single-stage power conversion shown in Figure 2.3(a), the AC grid voltage is fed to an AC-AC converter to ob-

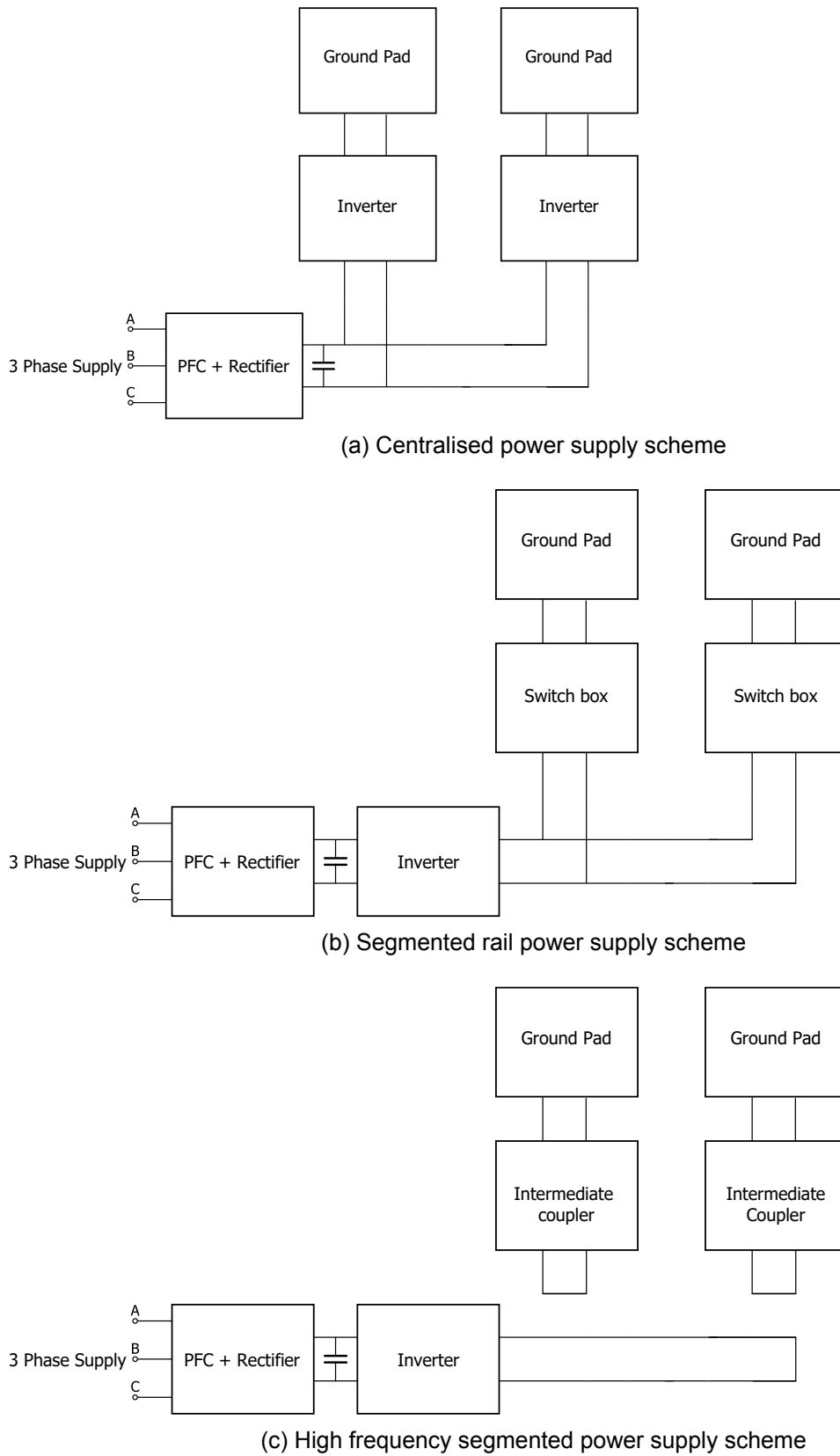


Figure 2.2: Grid side power supply architecture in a WPT system for EV charging [4].

Table 2.1: Summary of the power supply architectures used in IPT for EV charging.

Architecture	Constructional features	Advantages	Disdvantages
Centralised power supply scheme Figure 2.2(a)	The whole system is activated once the primary source is connected to the grid. All the system must be rated to withstand the full-power.	Simple in construction, low maintenance and installation cost. Less load pulsations as the system utilizes local energy storage. [4]	High-power rated components. Less efficient, and sensitive to parameter changes.
Segmented rail power supply scheme Figure 2.2(b)	Centralized power supply with switch boxes for activating each pad.	Smaller size and fewer inverter modules needed for the total number of pads. This reduces the power losses. Less sensitive.	High maintenance and construction cost. Control is complicated, as it requires a detector for selecting each pad.
High frequency segmented power supply scheme Figure 2.2(c)	The power supply is connected with an intermediate coupler to produce the high frequency output.	Primary pad and power supply are isolated easing the system's maintenance. The inverter's current amplitude is lower than the pad's one. The PE converter is distributed, so less lossy.	High frequency module produces high power loss.

tain the high-frequency resonant current. In the case of a two-stage power conversion shown in Figure 2.3(b), the grid voltage is fed to a rectifier with power factor correction that realize the AC-DC conversion. Then, an inverter outputs a high-frequency current to the compensation circuit from the previously rectified DC voltage. In the case of a three-stage conversion shown in Figure 2.3(c), the grid connection structure is similar to the two-stage conversion with an additional intermediate stage which regulates the DC voltage level by using a DC-DC converter.

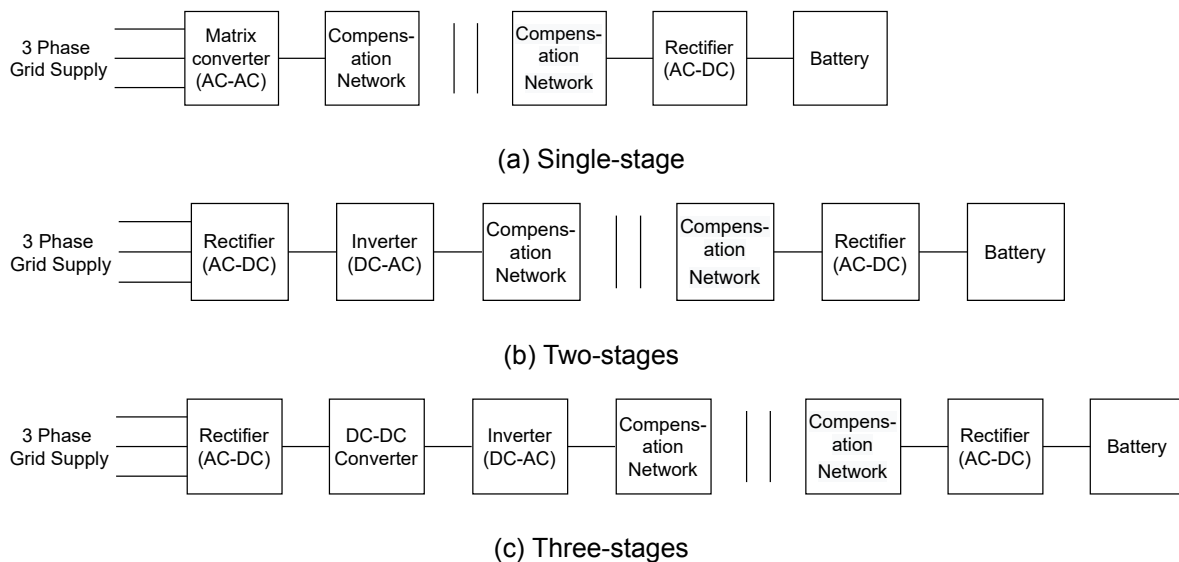


Figure 2.3: Grid-side power conversion stages for EV WPT-based charging systems.

At the output side, a rectifier is used to convert the high-frequency voltage picked up from the secondary coil. The resulting DC voltage is fed to the battery either directly or by using an additional DC-DC converter.

As a summary of Section 2.3.1 and Section 2.3.2, Table 2.2 shows the summary of various power electronics architecture used in IPT. The table highlights the number of stages and its architecture, the direction of flow of the power, semiconductor devices required, and the efficiency observed for different configurations. As it can be observed the number of semiconductor devices reduces with number of stages.

Table 2.2: Summary of the power electronics architectures used in IPT for EV charging.

References	Power supply architecture	No. of stages	Source behavior	Power flow	Primary semiconductor devices	Compensation network	Extra primary passive circuits	Other properties	Efficiency @ output power
[5]	IGBT based voltage controlled IPT module	3	VS	Unidirectional	6, 4, 4 switch modules for rectifier, inverter, and dc-dc converter respectively	C	Nil	Receiver side control & ZC switching control	96.4% @ 3 kW
[6],[7]	H-bridge converter	2	VSI	Bidirectional	4*Switching modules	LCL	DC link capacitor	PLL to control voltage angle	NA
[8]			CSI	Unidirectional	4*Diodes+4*switching module	LCC	DC inductor	Nil	NA
[9]	Conventional hybrid multiconverter	2	VSI	Bidirectional	(Number of primary levels-1)*MOSFET and 4 IGBT	CLC	Nil	Nil	92% @ full load
[10]	Hybrid multilevel converter - newly proposed	2	VSI	Bidirectional	(Number of primary levels-3)*MOSFET and 4 IGBT	CLC	Nil	Nil	92% @ maximum power level
[11],[12]	Multiphase converter	2	VSI	Unidirectional	6*switching module for rectifier +6*switching module for inverter	LCL	Inter-cell transformer	Phase frequency hybrid control	93.34% @ 1 kW
[13]	Resonant power supply	2	VS	Unidirectional	2*switching module for resonant supply+6 for rectifier	LC	Switching inductance	A step current injection model for ZVS frequency model	NA
[14]	Direct AC-AC converter	1	VSI	Depends on the load side converter	4*Bidirectional switches	LC	Nil	ZCS operation & Energy injection control	NA
[15]	Matrix Converter	1	VS	Unidirectional	4*bidirectional switching pair	RLC	Input filter	Nil	93% @ 980W
[16],[17]			VS	Bidirectional	Depends on the phase conversion type	LCL	Nil	Magnitude of power regulated by width of the Notch	NA

2.3.3. Compensation Networks

In any power electronic module, passive networks play a significant role in tuning the circuit. Likewise, in WPT, the need for compensation networks made of passive elements to regulate power transfer and tuning the primary circuit to the secondary is necessary. Due to the existence of high magnetizing and leakage inductances in the primary and secondary coils, the WPT system would require a high VA rating from source to transfer active power to the load [4]. The higher VA rating from input source would bring down the efficiency and lifetime of power electronic circuit. To avoid this circulation of reactive current, compensation networks are connected in either series or parallel to compensate for the leakage inductance. Apart from compensating for the reactive power, the compensation networks also have either a voltage-source or a current-source behavior that is independent of the load.

According to [4], the main properties that a compensation network must comply with are:

- maximize the power transfer and the power supplied to the secondary converter;
- minimize the power supply VA rating and improve the efficiency of the complete system;
- have high misalignment tolerance;
- tolerate or avoid the bifurcation phenomenon;
- provide a constant voltage or current to the output depending on the system requirements.

The basic compensation networks are generally classified into four types depending on the placement of the passive elements. The series-series (S-S) compensation is shown in Figure 2.4(a), where one compensation capacitor is connected in series with the main coil at both primary and secondary side. In the series-parallel (S-P) compensation as shown in Figure 2.4(b), the primary compensation capacitor is connected in series with the primary coil, but the secondary compensation capacitor is connected in parallel with the secondary coil. The parallel-series (P-S) compensation as shown in Figure 2.4(c), is the converse of the S-P compensation where the primary capacitor is parallelly connected while the secondary capacitor is placed in series. Finally, the parallel-parallel (P-P) compensation as shown in Figure 2.4(d), is the converse of the S-S design where both the primary and secondary compensation capacitors are connected in parallel to the coupled coils.

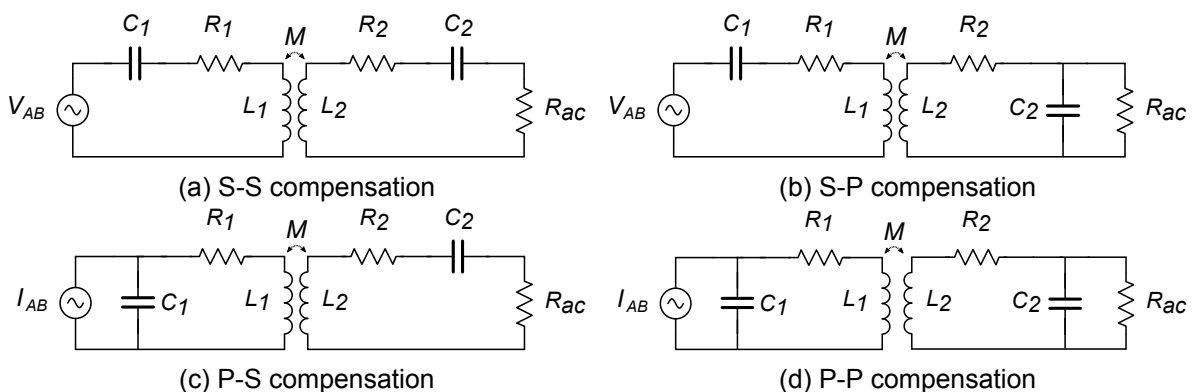


Figure 2.4: Equivalent circuit of an IPT system with magnetic resonant coupling

2.3.4. Mathematical analysis of the S-S compensation network

From the equivalent circuit shown in Figure 2.4(a), the maximum deliverable output power and the power transfer efficiency can be deduced from the circuit equations as explained in [15].

1) Load power analysis:

As seen in the equivalent circuit, the primary-side RLC circuit is in series with the parallel combination of the mutual inductance and the secondary RLC network. The equivalent input impedance Z_{in} seen from the primary voltage source is

$$Z_{in} = R_1 + j\omega L_1 + \frac{1}{j\omega C_1} + \frac{M^2 \omega^2}{R_2 + j\omega L_2 + \frac{1}{j\omega C_2} + R_{ac}} \quad (2.1)$$

where R_1 is the primary equivalent series resistance, L_1 is the self inductance of the primary coil, C_1 is the primary compensation capacitance, M is mutual inductance between the primary and secondary coils, R_2 is the equivalent series secondary resistance, L_2 is the self inductance of the secondary coil, C_2 is the secondary compensation capacitance, $\omega = 2\pi f$ is the angular frequency, and R_{ac} is equivalent load resistance.

At the resonant angular frequency $\omega = \omega_0$, the reactance given by the capacitance and the inductance must cancel each other out. Therefore, the resulting equivalent Z_{in} observed in the system is purely resistive and can be expressed as

$$Z_{in} = R_1 + \frac{M^2(\omega_0)^2}{R_2 + R_{ac}} \quad (2.2)$$

Additionally, from the Kirchhoff's voltage law, the equations of the S-S compensation can be written as:

$$\begin{cases} V_{AB} = (R_1 + j\omega L_1 + \frac{1}{j\omega C_1})I_1 + j\omega M I_2 \\ 0 = (R_2 + j\omega L_2 + \frac{1}{j\omega C_2} + R_{ac})I_2 + j\omega M I_1 \end{cases} \quad (2.3)$$

where V_{AB} is the primary side source voltage, I_1 is the primary side current, and I_2 is the secondary side current. The relationship between I_1 and I_2 at the resonance can be found from (2.3), which is

$$I_1 = \frac{R_2 + R_{ac}}{j\omega_0 M} \cdot I_2 \quad (2.4)$$

Therefore, I_2 can be written as

$$I_2 = \frac{j\omega_0 M}{R_2 + R_{ac}} \cdot I_1 = \frac{j\omega_0 M}{R_2 + R_{ac}} \cdot \frac{V_{AB}}{Z_1} \quad (2.5)$$

Since the load is resistive, the output power is given by

$$\begin{aligned} P_{out} &= \left(\frac{I_2}{\sqrt{2}}\right)^2 \cdot R_{ac} \\ &= \frac{R_{ac}}{2} \cdot \left(\frac{V_{AB}}{\omega_0 M + \frac{R_1(R_2 + R_{ac})}{\omega_0 M}}\right)^2 \end{aligned} \quad (2.6)$$

(2.6) shows that the output power P_{out} depends on the mutual inductance M and the load resistance R_{ac} . The mutual inductance $M = k\sqrt{L_1 L_2}$ depends on the coils' self inductance under consideration and the coupling factor k which varies with the distance between the windings.

Hence the coupling coefficient and the coils' quality factor that is function of the inductance ($Q = \frac{\omega L}{R}$) determines the amount of power transferred to the secondary circuit. Differentiating the load power with respect to R_{ac} or M gives the load resistance and mutual inductance at which the maximum power is transferred, respectively.

2) Efficiency analysis:

The ratio between the output power and the input power is defined as efficiency. According to (2.6), the output power or load power depends on the secondary current and load resistance. The input power depends on the output power and the resistive losses in both the primary and the secondary circuits at resonant angular frequency. Therefore, the efficiency of the circuit depicted in Fig 1.1 is given by

$$\eta = \frac{I_2^2 R_{ac}}{I_2^2 R_{ac} + I_1^2 R_1 + I_2^2 R_2} \quad (2.7)$$

Dividing both the numerator and the denominator by the numerator term in (2.7):

$$\eta = \frac{1}{1 + \frac{I_1^2 R_1}{I_2^2 R_{ac}} + \frac{R_2}{R_{ac}}} \quad (2.8)$$

Substituting (2.4) in (2.8) results in

$$\eta = \frac{1}{1 + \left(\frac{R_2 R_{ac}}{\omega_0 M}\right)^2 \frac{R_1}{R_{ac}} + \frac{R_2}{R_{ac}}} \quad (2.9)$$

(2.9) shows that the efficiency depends on mutual inductance and as well the load resistance. Higher mutual inductance corresponds to a reduced distance between the two coils, which leads to a higher efficiency. As well, the optimal tuning of the load resistance leads to higher efficiency. This optimum load resistance can be found by differentiating the efficiency with respect to the load resistance.

2.3.5. Coupled Pads

Coupled magnetic pads form the basis of an IPT system. These coupling pads enable the transfer of power from the source to the load without any electrical connection. Coupling pads consists of coupled inductors with a considerable air gap in between them. The coupling factor between the two inductors indicates the strength of the mutual magnetic field that is linked to both inductors. This concept is known as mutual coupling. The magnetic pad is composed of a Litz-wire winding placed over a ferromagnetic material that has a certain amount of aluminium shielding at the opposite side. As summarized in Table 2.3, there are mainly six different types of coupling pads used in EV wireless charging .

The magnetic flux determines the amplitude of the voltage that gets induced in a conductor located in the proximity. Depending on the pad geometry, the magnetic flux that comes out of pad can be either single-ended, also called non-polarized, or double-ended, also called polarized. In case of non-polarised, for instance the circular coil, there is only one equivalent magnetic pole. The field goes out from the center and comes in through the sides of the ferrites. The field distribution is more vertical. In case of polarised, for instance DD coil, there are two poles, and hence the field goes out from the center of one pole and comes in through the center of the other pole. Here, the direction of field is more horizontal. Effect of the shielding on coupling coefficient is high for polarized as the field from the shield (which is

Table 2.3: Summary of the coupling pad architectures used in IPT for EV charging [4].

Pad structure	Equivalent number of coils	Magnetic flux	Effect of the shielding on the coupling coefficient
Circular/Rectangular Pad Figure 2.5(a)	One	Non-Polarized	Low
Flux pipe Figure 2.5(b)	One	Polarized	High
DD coil Figure 2.5(c)	One	Polarized	High
DDQ coil Figure 2.5(d)	Two	Polarized	High
Bipolar pad Figure 2.5(e)	Two	Polarized	High
Tripolar pad Figure 2.5(f)	Three	Non-Polarized	Low

plane from the backside of the ferrite) is parallel to the field of the pad. Single-ended model is more efficient, as well the flux pattern helps in reducing the leakage flux. Hence, circular coils and its variants like rectangular are highly efficient and easy to design. Although, circular pads have a low value of k and as well the tolerance towards misalignment is very poor, these pads are chosen widely due its single-ended flux distribution attribute and as well the simplicity in its design. Tripolar pads are three-coil couplers where all the three coils are mutually decoupled and, this geometry allows high misalignment tolerance. The mutual decoupling paves for high coupling factor. Although it has many advantages as mentioned in the Table 2.3, the need for three inverters to operate the three decoupled coils makes the system complex and costly. To conclude, the circular pad and tripolar pads stand out to be a better choice.

2.3.6. Control of IPT systems

Control becomes a prominent part of any IPT system. Essential control is implemented to ensure an efficient power transfer to the load at the required power level. Moreover, a safe IPT must be ensured. This is realized though a foreign object detection (FOD) system, and a control that limits the human exposure to harmful fields. To achieve so, the communication between the coupled pads might be needed. On the whole, the control of a WPT can be divided into five parts namely power control, maximum efficiency tracking, FOD and vehicle detection, misalignment detection, and communication [3].

1) Power control:

Power control focuses on delivering the required output power level to the load. Based on its placement, the power control is divided into three categories, namely, primary-side control, secondary-side control, and dual control. In the primary-side control, the data related to the battery voltage, current and state of charge are fed to the primary via a wireless communication network. Based on the data received, the closed-loop control in the primary side tunes the input voltage source. In the secondary-side control, synchronous rectification is used in secondary side to control constant current and is usually used in applications where multiple

pick-up coils are used as in the case of dynamic charging. In the dual-sided control, the pri-

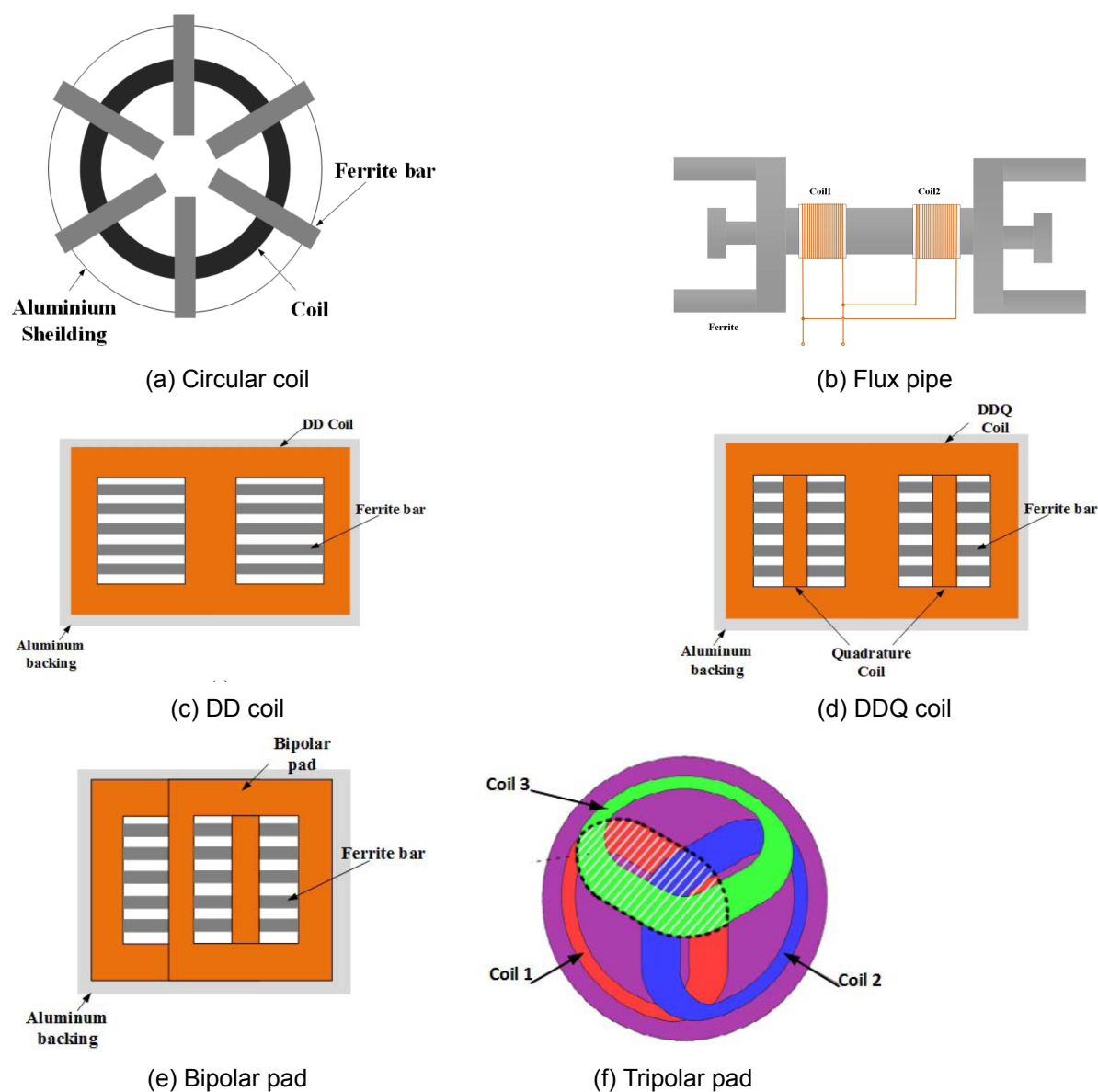


Figure 2.5: Coupling pads for WPT based charging system for EVs [4].

mary side and secondary side are simultaneously controlled so as to control the power flow. Additional dc-dc converters can be added in both the primary and secondary side to regulate the voltage to the required level [3].

2) Efficiency tracking:

Despite the variation in load or coupling coefficient, this control ensures that maximum efficiency is maintained throughout the operation. This control can be labelled into three groups. The first group deals with the impedance matching technique during the load variation, where the impedance matching system converts the load impedance to optimal impedance during load and magnetic coupling variations. The second group focuses on attaining maximum efficiency during load variation by integrating the output control and the load variation. The third group focuses on reducing the input reactive power by controlling the input to attain maximum efficiency [3].

3) FOD and vehicle detection:

Interference of foreign objects with the magnetic coils of the WPT system leads to the production of unnecessary fields if the source is a magnet, while it leads to heat production if the source is a metal. These fields and excessive heat may cause turmoil to the whole system and as well it can have effects on living bodies. To eradicate the adverse condition caused to the system, FOD is a requirement for any WPT system. The primary pads of the WPT must be activated only while the vehicle is approaching to obtain high efficiency of the system and as well to reduce the field radiations. To ensure that the primary pads are activated only when a vehicle is approaching, a vehicle detection sensor is required. This sensor guarantees that the power is supplied to the primary pad only when the secondary pad is present [3].

4) Misalignment

The coupling coefficient is affected directly when the primary pads and secondary pads are not in alignment. As said earlier, the coupling coefficient directs the amount of power that gets transferred, which thereby affects the system efficiency. Hence any misalignment would cause a reduction in the system's efficiency and the amount of magnetic field that the secondary pad receives. The WPT system must include a misalignment detection system to ensure maximum power transfer and system efficiency for the specific magnetic coupling condition [3].

5) Communication

Communication plays a pivotal role in connecting the primary side and the vehicle. To ensure the reliable and secure operation of the WPT system, timely data exchange between primary and secondary is a must. Hereby, the primary criteria is that a communication system must possess low latency, and at the least, medium-range coverage [3].

2.3.7. Standardization of IPT systems for EV charging

The design of WPT must follow recommended standards that are approved by the scientific committees across the field. Static WPT charging has a complete framework of standardisation while the dynamic WPT is still under construction. Static WPT follows the guideline of SAE J2954 for the design of magnetic couplers, compensation circuits, electrical constraints of the vehicle under consideration, while the ICNIRP 2010 is considered for the human exposure to electromagnetic fields (EMF). The latter provides the EMF limits for the considered operating frequency. These considerations are unavoidable during the design of a WPT system, and as well the human safety. Apart from SAE J2954, also IEC 61980 focuses on the IPT charging of light-duty vehicle.

In the original draft of SAE J2954, various design requirements and principles are elucidated, which encompasses the optimum frequency range, distance classes, power level classes and so forth [3]. In general, the WPT systems can be classified into four types based on their input power levels, namely WPT1 (3.7 kVA), WPT2 (7.7 kVA), WPT3 (11.1 kVA) and WPT4 (22 kVA). The recommended frequency of operation for efficient operation ranges from 79 kHz to 90 kHz, where 85 kHz is selected as nominal operating frequency. At relatively high frequency, the usage of Litz wire reduces the AC losses of the coupled coils. The allowed distance between the ground and surface of the secondary coil is categorized into three classes, namely Z1 for the distance of (100-150) mm, Z2 for the distance of (140-210) mm, and Z3 for the distance of (170-250) mm [3].

3

AC-AC Matrix Converters

This chapter intends to be an overview of the matrix converter. This chapter discusses primarily the circuit model and the working principle of the matrix converter. After that, the characteristics and possible implementations of four-quadrant switches are summarized. Finally, an overview of the commutation strategies is given.

3.1. Matrix Converter - Evolution, Circuit and its Working principle

The conversion and control of energy are perhaps the main features of electrical engineering applications. As of late, these applications are characterized by the utilization of active semiconductor devices and energy-storing components like capacitors and inductors. A few converter families have been created such as rectifiers, inverters, choppers, cyclo converters, and so on. Every one of these families has its benefits and constraints. The primary benefit of power converters is the high efficiency that can be accomplished. Among these topologies, this research focuses on the AC-to-AC converters that are commonly called matrix converters. A matrix converter is an array of four-quadrant switches, which are the fundamental power components. It interconnects straightforwardly an AC single-phase or three-phase power supply to another AC single phase or three-phase load with different operating frequency, without utilizing any DC connection or large energy storage components and, in this manner, it is known as the all-silicon solution [18]. The main qualities of the matrix converter are:

1. a relatively simple and minimal power circuit;
2. the generation of a load voltage with arbitrary amplitude and frequency.

These profoundly appealing characteristics are the reason of the large interest in this topology. The implementation of this converter begins with the early work of Venturini and Alesina [2]. They introduced the power circuit of the converter as a matrix of four-quadrant power switches and they presented the term 'matrix converter'.

Generally, a matrix converter is a single-stage converter with $m \times n$ four-quadrant power switches which intends to interface an m -phase voltage source to an n -phase load. In other words, the matrix converter is an AC-AC converter which can convert power from desired m phases to desired n phases. Hereby, the 3×3 matrix converter model is taken as an example to explain the various components present in the circuit schematic of a matrix converter.

The 3×3 matrix converter, shown in 3.1, is the basic converter module encompassing the filter circuits at the input side, the RL load at the output, 9 pairs of switches sets connecting

the source and the load. Each switch shown is a four quadrant power switches. The matrix converter has a voltage source as an input, and therefore, the input terminals must not be short-circuited. Additionally, since generally the load has an inductive nature, the load stage should never be opened. The filter at the input side is composed of an inductor connected in series to a resistor and a capacitor. The main purpose of this filter is to filter out the high frequency components of the input current thereby ensuring an almost sinusoidal-like current and, as well, to avoid the overvoltage due to the fast commutation of the currents. Due to presence of a filter capacitance at the input side, only one switch at the time can be closed in the same vertical leg of the matrix converter of Figure 3.1. Moreover, since an inductor is also present, to maintain a continuous flow of current, at least one switch must be closed in each leg.

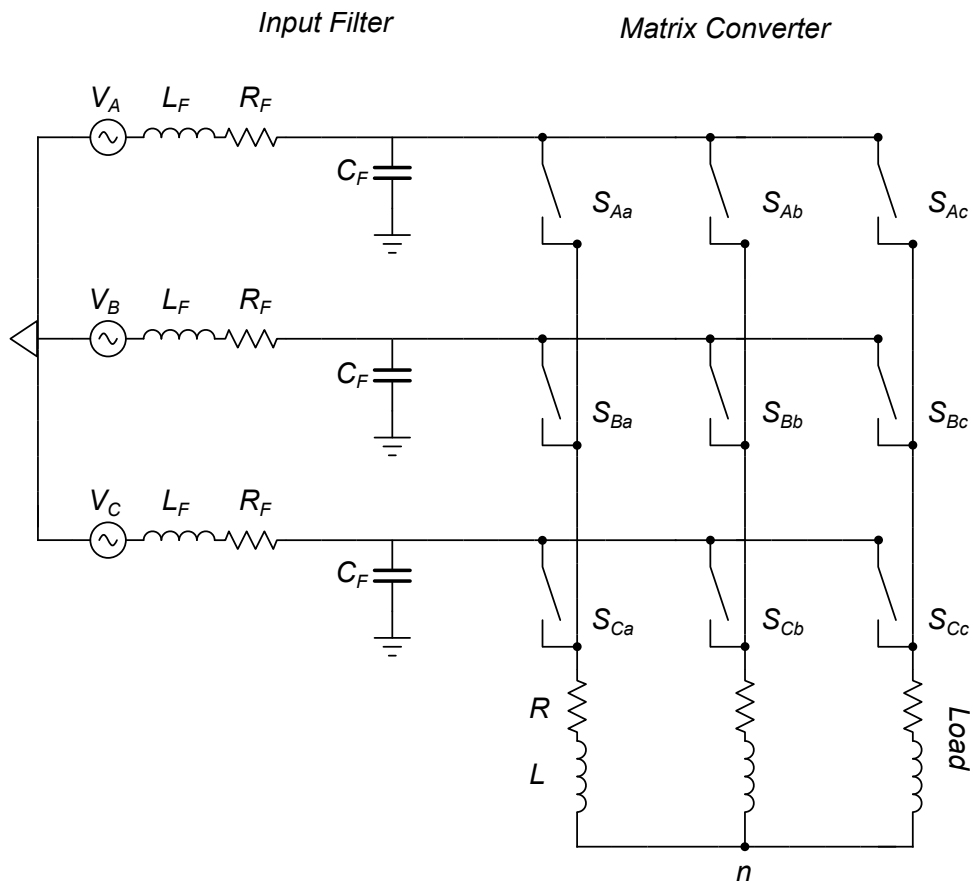


Figure 3.1: Three Phase Matrix Converter.

3.2. Four-quadrant Switch

As said earlier, a 3 x 3 matrix converter has 18 switches and 9 cells. So each cell has two switches connected in anti-parallel. This phenomenon leads to a concept of four-quadrant operational switch, which is capable of blocking voltage and conducting current in both the directions [19]. In order to achieve the blocking and the conduction of voltage and current in both directions, the discrete available switches must be connected in such a manner so as to accomplish the four-quadrant configuration. In practice, there are three possible four-quadrant switch configurations as shown in Figure 3.2: diode bridge four-quadrant switch cell, common-source anti-parallel MOSFETs, common-drain anti-parallel MOSFETs.

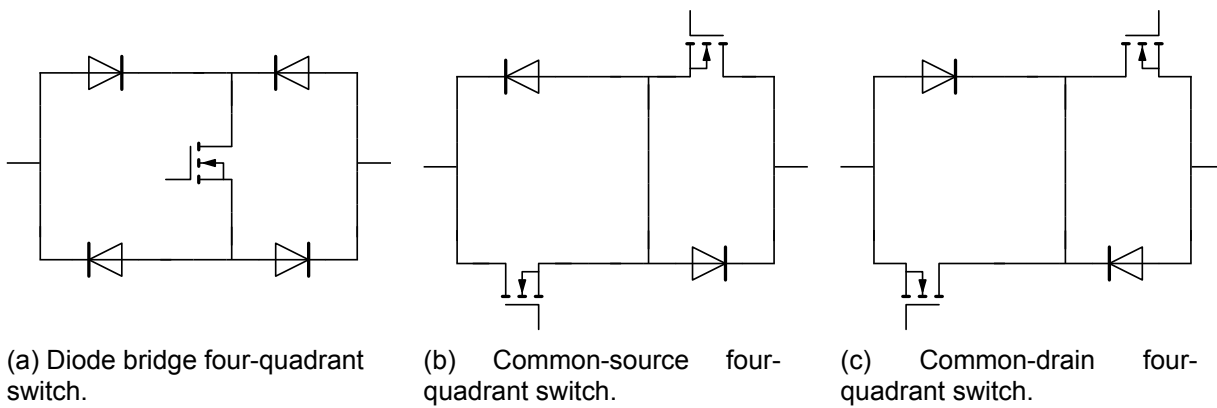


Figure 3.2: Possible configurations of a four-quadrant switch.

The diode bridge four-quadrant switch cell consists of a central MOSFET surrounded by four diodes as shown in 3.2(a). The device losses are relatively high as the MOSFET and two diodes conduct simultaneously. Since both the current directions are carried by the central MOSFET, the gate driver required is just one per switch cell.

The common-source four-quadrant switch consists of two MOSFETs and two diodes connected in anti-parallel as shown in 3.2(b). This ensures independent control of the current direction. The two MOSFETs require an isolated gate drive circuit. However, in the case of a common-source module, both devices are driven with regards to same voltage, that is the common-source point.

The common-drain four-quadrant switch is similar to the previous one with the exception that the common voltage point is drain port as shown in 3.2(c). However, this is not feasible in reality largely due to the presence of stray inductances in between the commutation cells leading to stability issues.

So to conclude, the common-source module is the best practical choice. Anyhow, any switching module possessing reverse voltage blocking capability can be used to build a four-quadrant switch by placing them in anti-parallel.

3.3. Commutation

The commutation is a process of turning off the switch and, as a result, removing the switching current completely. In case of a matrix converter, it is cumbersome to achieve commutation between switches since there are no freewheeling path. According to [20], in order to control the switching, two basic requirements must always be fulfilled. First, two switches must not be turned on at the same time in the same leg as shown in 4.8(a), as it would lead to short circuit of the capacitor voltage and this would lead to extreme current rise and, eventually, to the destruction of the converter. Secondly, the two switches of the same leg must not be turned off at the same time as shown in 4.8(b), as it would lead to open circuit at the load side causing over-voltage due to the absence of path for the inductive load current.

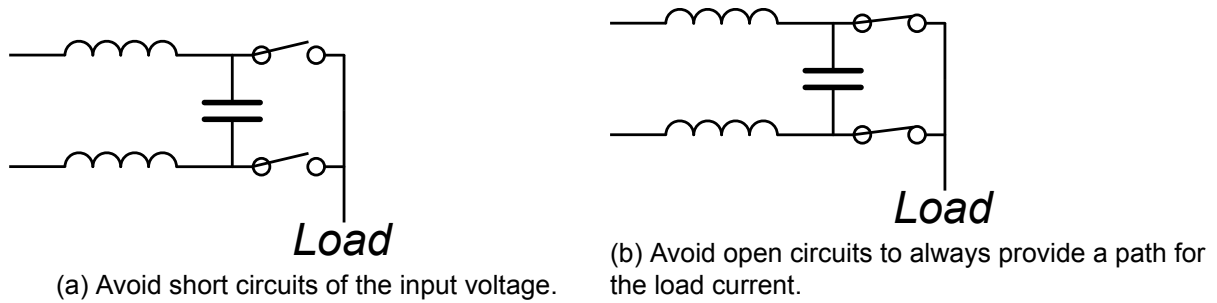


Figure 3.3: Commutation strategies requirements.

The switching strategy can be controlled to achieve high efficiency. In the case of hard switching during turn-on and turn-off, both the voltage and the current across the switch have large amplitude for a relatively short time, causing noise and thereby losses. On the contrary, soft switching uses a specific operation to attain zero voltage or zero current switching. As the turn-on and turn-off occur at either zero or close to zero voltage and current, the switching noise and losses reduces drastically.

The switching strategy to attain soft switching is explained in detail in Chapter 4 and 5.

3.4. Input filters

Filters at the input side are mandatory during the design of matrix converters to reduce the input current harmonics. The requirements for the input filter module are as follows [21]:

- To have cut-off frequency higher than the grid frequency and as well lower than the switching frequency of the converter.
- To ensure minimum voltage drop across the filter inductance so that the voltage transfer ratio between input and output are maintained.
- To ensure the size and the weight of the capacitor and inductors are minimum.

3.5. Matrix converters in WPT applications

Matrix converters can convert the grid side AC voltage to a high frequency AC voltage. Using matrix converters for wireless power transfer systems are advantageous as the conversion stage in the grid side is just one instead of the conventional two stages as shown in Chapter 4 and 5. Moreover, the DC link capacitor size is appreciably reduced.

In literature, there are few papers which focuses on matrix converter based wireless power transfer system for electric vehicle application.

[17] describes a single phase matrix converter which acts as an ignition for the wireless power transfer system. The paper provides a steady state mathematical modelling and explains the effect of variation in phase angle between the primary side converter and the secondary side converter for the bi-directional flow of power. When the phase angle is leading between the primary side converter and secondary side converter, the system transfers power from the vehicle pick up to the grid and when the phase angle is lagging, power is transferred from the grid to the vehicle. Finally the simulation verification was provided to support the analytical equations derived.

[16] briefs about the design of the three phase matrix converter for the wireless power transfer of power for an electric vehicle applications. The three phase grid power supply provides in the necessary high frequency active element which drives the primary pick up coil that resonates with the secondary coil and powers up the battery load. The simulation verification

is provided to support the mathematical expression and as well the effect on changing the phase angle and width of the notch on magnitude of power.

[22] lists various possible architecture for three phase matrix converter based power transfer model. Detailed analysis of isolated matrix type star rectifier where the matrix converters are connected in star and the output of the converter is fed to three transformer models whose secondary is connected in series. The control strategy to regulate the balance in the grid side system and the load power are described and simulation verification is provided.

[23] describes the three phase modular isolated matrix type star or delta rectifier. This paper provides the working principle of the converter and as well gives a detailed design of various necessary parameters. This paper provides a better design of matrix converter in the form of a rectifier followed by a H-bridge converter.

[24] describes the three phase modular isolated indirect type matrix converter. The detailed operation principle with control strategies is given. The modulation techniques and the effects of symmetric and asymmetric modulation techniques are proposed alongside providing the prototype design.

The system specified in [17] and [16] are both operated at a frequency of 20 kHz. The system analysed in this thesis is designed at center operating frequency of 85 kHz. Additionally, control strategy is introduced to balance the input current and the output power in case of three phase system.

4

Single Phase to Single Phase Matrix Converter

This chapter deals with the analysis of single-phase to single-phase matrix converters for WPT applications. A description of the single-phase to single-phase matrix converter implementation, followed by the creation of the gating pulses as to attain soft switching. The converter is evaluated with a mathematical modelling for different design constraints and considering the battery cycle. Finally, evaluating the grid side current harmonics with the available standard.

4.1. Implementation

The AC grid voltage at the frequency of 50 Hz can be converted to a desired high frequency AC load through a matrix converter. The single-phase matrix converter module possess 8 switches in total, with 4 switches in each leg. The grid voltage can be connected to different configurations of the converter to attain high frequency AC voltage at the output side. Hereby, two different configurations were analysed:

1. four-quadrant switches-based model;
2. rectifier followed by a H-bridge-based model.

4.1.1. Four-quadrant switches-based model

The 8 switches are split into 4 switching cells, where two of them are part of each leg. Hence, the configuration looks similar to an inverter bridge with two legs in which each switching cell is composed of a four-quadrant switch. This topology is represented in Figure 4.1. The positive polarity of the AC voltage from the grid is fed to the drain of the upper leg MOSFETs as shown in Figure 4.1 while the negative polarity is connected to the drain of the lower leg MOSFETs which is grounded as shown in Figure 4.1. The source of one switch is connected to the source of the other switch to attain four-quadrant operation. The output is taken from the drain to drain connections (A1 and B1) of two legs as shown in Figure 4.1. As seen in Figure 4.1, the MOSFET and diode are connected in anti-parallel. Only four switches are conducting while the other four switches commutate at the switching frequency during each half cycle of the input voltage pulse. Hence, the switching pulses have to be developed separately for the positive and negative half-wave of input voltage. During the positive pulse of the input voltage, S1, S3, S5 and S7 conduct while the others conduct during the negative cycle of the voltage source.

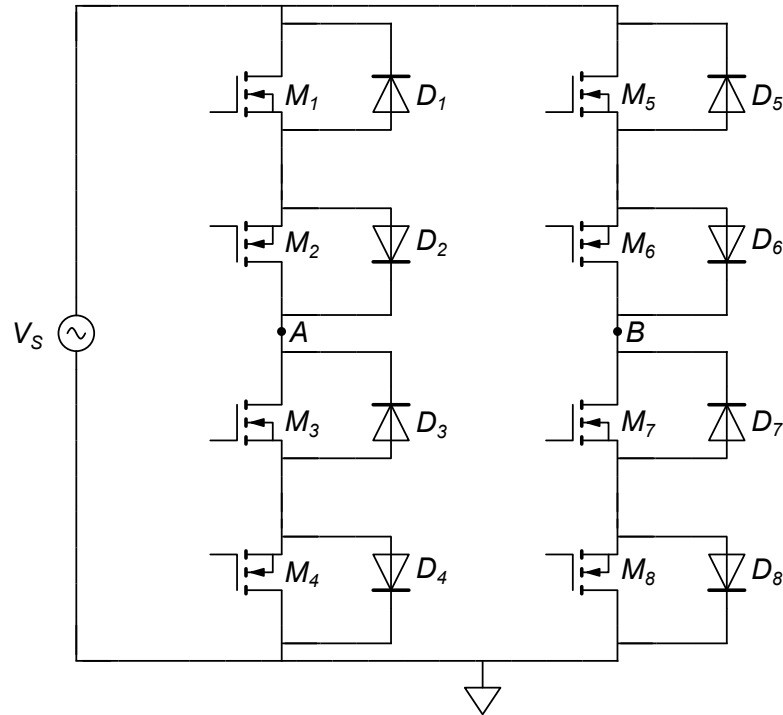
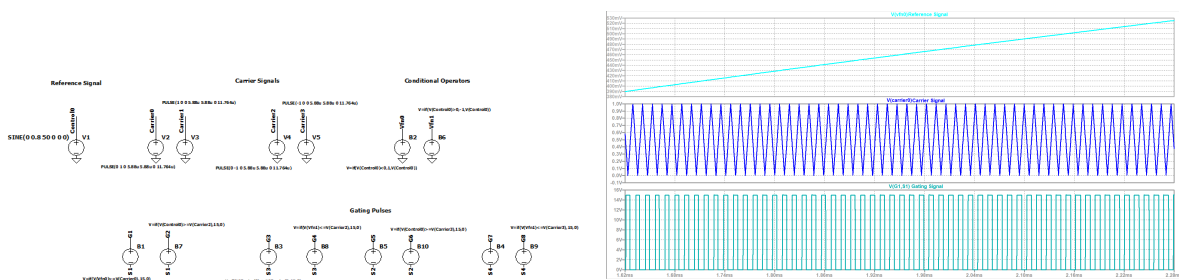


Figure 4.1: Four quadrant operation switch configuration of Matrix Converter

The comparison of carrier signals with reference signals with optimum limits fetches proper gate pulses for each switch. The reference is the sinusoidal voltage with its amplitude taken to be 0.8 and the carrier signals are triangular voltages with amplitude 1. There are four carrier signals used as shown in Figure 4.2, two for each cycle of reference voltage. The conditional operators are used so that the four non-operating switches during each cycle are turned on throughout. For instance, the switch S2, S4, S6 and S8 are kept conducting during the positive cycle of reference signal as shown in Figure 4.3(a). The gating pulse condition for each switches is as shown in Figure 4.2 and the pulses for all the eight switches obtained as shown in Figure 4.3(b). The frequency of the carrier wave is set at the resonant tank frequency of 85 KHz while the reference signal frequency is 50 Hz.



(a) Model.

(b) Gating pulse. X-axis depicts the time in seconds (sec) and Y-axis depicts the voltage in volt (V).

Figure 4.2: Gating pulses for single-phase four-quadrant switch configuration of the matrix converter.

As said before, the gating pulse obtained in Figure 4.3(a) confirms the fact that only 4 switches operate at the 85 kHz switching frequency during each half cycle of the 50 Hz input voltage while other four stays constantly on.

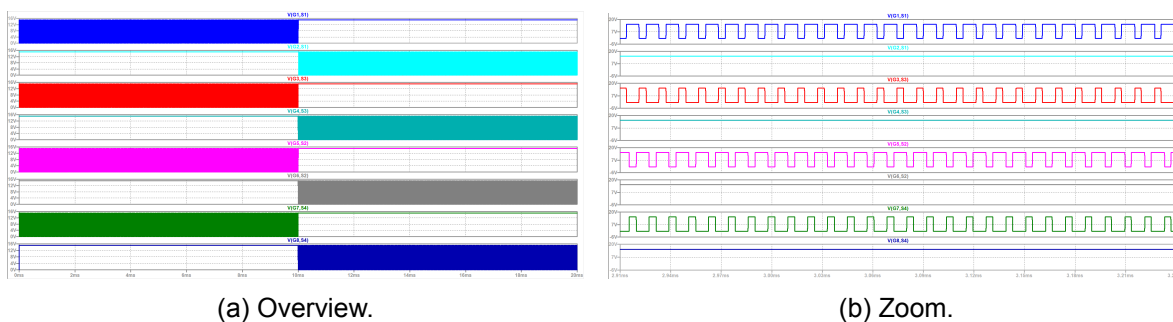


Figure 4.3: Gating pulses for single-phase four-quadrant switch configuration of the matrix converter. X-axis depicts the time in seconds (sec) and Y-axis depicts the voltage in volt (V).

The output voltage of the converter obtained for the applied gating pulses is shown in Figure 4.4. It can be seen that the obtained voltage is a 50 Hz cycle with each cycle constituting of 1700 cycles at the frequency of 85 kHz. It can be concluded from this waveform that the configuration and the gating pulse generation are feasible.

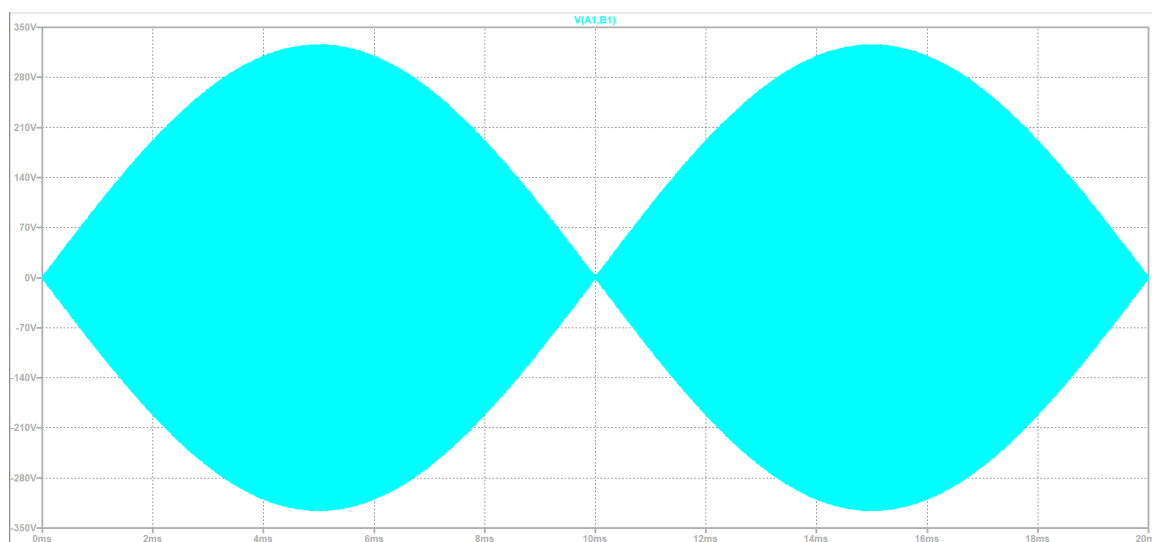


Figure 4.4: Converter output voltage (measured at terminal AB as show in Figure 4.1) for single-phase four-quadrant switch configuration of the matrix converter. X-axis depicts the time in seconds (sec) and Y-axis depicts the voltage in volt (V).

4.1.2. Rectifier and H-bridge-based model

The rectifier and H-bridge-based model modifies the configuration of the switching cells compared to the four-quadrant switch-based model. The eight switches are split into two bridges with four switches. One bridge is used as a rectifier to obtain just the positive half-wave of the sinusoidal grid voltage. The remaining four switches acts as a H-bridge converter which converts the half-wave rectified voltage to the high frequency AC wave. As seen in Figure 4.5, the 50 Hz grid voltage is fed to the rectifier, the rectified output pulse is fed to the the H-bridge converter module which produces a high-frequency, switching frequency, AC pulse. The configuration specified in Figure 4.5 is relatively easier to construct and to control when compared to the one specified in Figure 4.1. Four-quadrant switches-based model is quite complex to construct, the design of gate drive circuit is tedious, and lastly, the model wasn't able to attain soft switching at the operating condition. The gate drivers were designed on a conditional basis for positive and negative cycle of the source pulse. The converter module was not able

to attain soft switching under normal operating conditions, even with the introduction of delay time and dead time. All the eight were not able to operate in ZVS condition at any instant in time. Hence, in the forthcoming sections of this chapter, Figure 4.5 is used for this analysis.

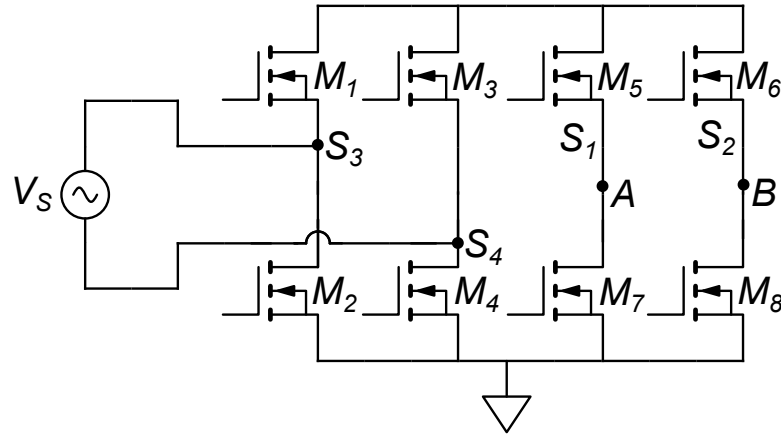


Figure 4.5: Rectifier followed by a H-bridge configuration as matrix converter.

The gating pulses for rectifier and H-bridge converter are designed as shown in Figure 4.6. The gating pulses, instead of carrier waveform based generation, operating each leg of the bridge at 50% duty cycle or (50-time delay)% generates the same result as seen in carrier-based generation. In the case of the rectifier, conditional operator based generation of pulses is opted while in case of H-bridge, duty cycle based generation of pulses is preferred. Diode bridge rectifier can be used and or preferred instead of MOSFET-based rectifier bridge model for the easier controllability. The pulses for H-bridge as seen in Figure 4.6 are defined for a switching frequency of about 85 kHz, and a delay time of 100 ns is specified.

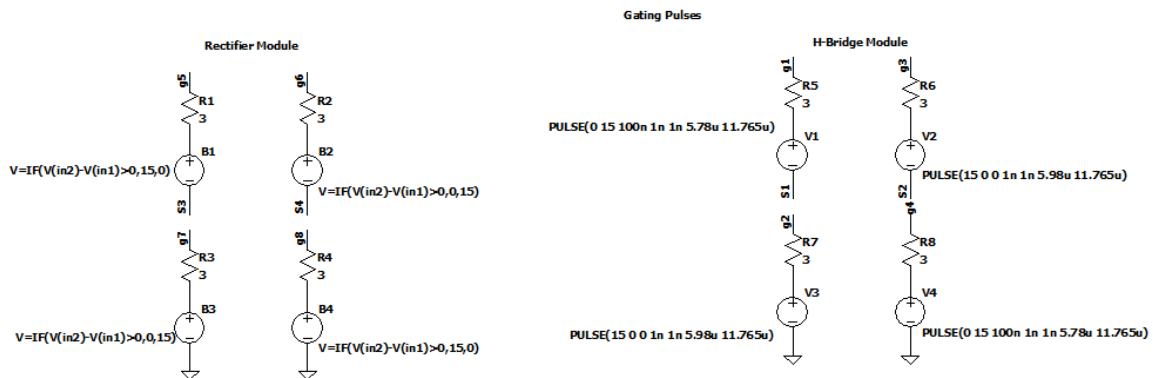


Figure 4.6: Gating pulses for single phase rectifier with H-bridge switch configuration of the matrix converter.

The pulses for rectifier bridge is obtained as shown in Figure 4.7. During the positive pulse of the input sine voltage, M1 and M4 conduct, while M2 and M3 are kept off. The positive pulse at the input thus stays positive with the same amplitude at the output side. During the negative pulse of input voltage, M2 and M3 conduct, while M1 and M4 are turned off. The negative

pulse traverses through switch M3 and M2 via load and produces a positive pulses at the load. Thus the voltage obtained at the H-bridge stays positive unlike four quadrant switch configuration. Hence, the switching logic can be designed for only the positive pulse of the input voltage.

The gating pulses for the H-bridge are designed in such a way as to obtain a desired frequency sinusoidal waveform. So the pulses are going to have a period of $1/f$. As shown in Figure 4.6, the ON-time for G1 and G4 are provided to be $5.78 \mu\text{s}$ instead of $5.88 \mu\text{s}$ in order to introduce a short dead time between the switches.

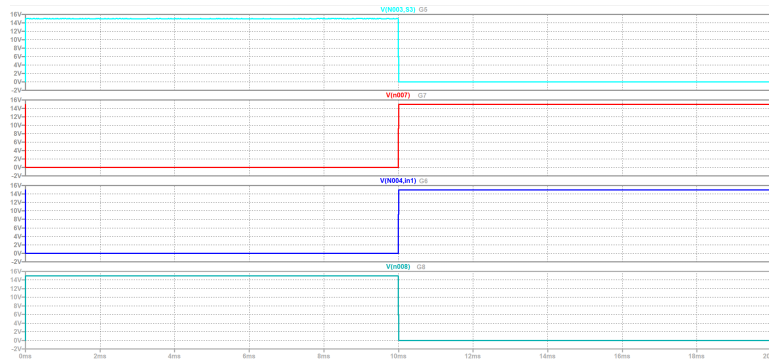
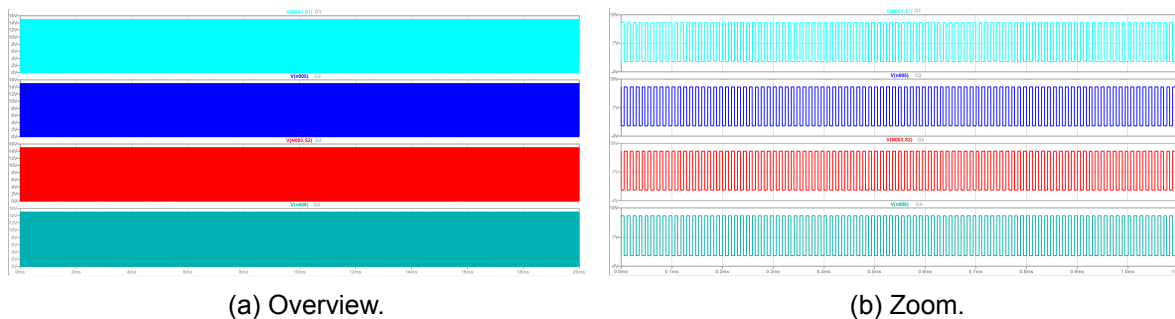


Figure 4.7: Gating pulse: delay and dead time. X-axis depicts the time in seconds (sec) and Y-axis depicts the voltage in volt (V).

As seen in Figure 4.8(b), the gate pulses G2 and G3 are shifted 180 degrees apart with regards to gate pulses G1 and G4. The resultant waveform at the output of the rectifier followed by H-bridge matrix converter is as shown in Figure 4.9 and it is similar to Figure 4.4.



(a) Overview.

(b) Zoom.

Figure 4.8: Gating pulse signals for single-phase rectifier with H-bridge matrix converter. X-axis depicts the time in seconds (sec) and Y-axis depicts the voltage in volt (V).

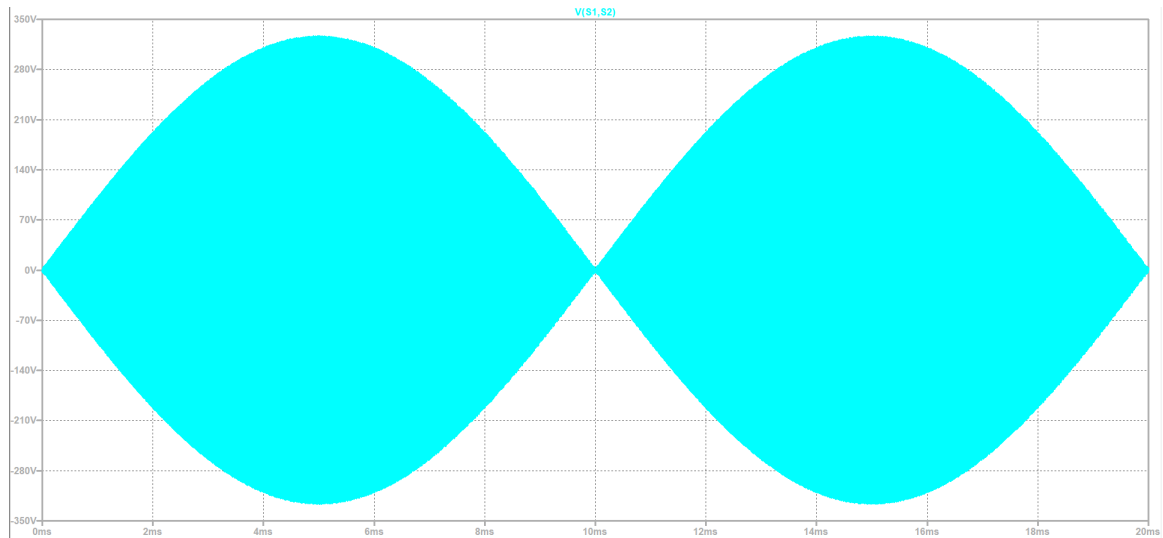


Figure 4.9: Output voltage of the single-phase rectifier with H-bridge matrix converter. X-axis depicts the time in seconds (sec) and Y-axis depicts the voltage in volt (V).

4.2. Single phase matrix converter for WPT in EV charging

The Indirect Matrix Converter (Rectifier followed by H-bridge Converter) is preferred for the further analysis as the control of switching signals and the converter control is simple. The converter output port is connected to the primary resonant tank which is then mutually coupled with the secondary resonant tank. The output from secondary resonant tank is fed to the converter to convert the high frequency AC current to a direct current as shown in Figure 4.10. The resonant shown in Figure 4.10, is designed for the centre operating frequency of 85 KHz as suggested from the standard SAE J2954 [25].

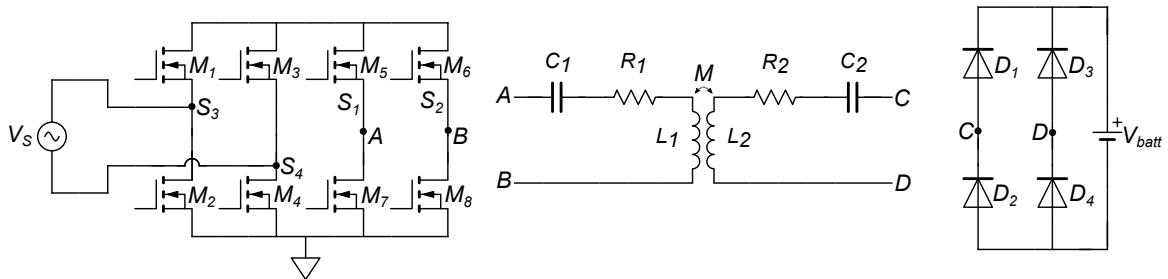


Figure 4.10: Single-phase matrix converter with the resonant tank and battery load.

The parameters of the coil are chosen as the one available in the lab. The coil available in the lab is a DD coil with L_1 being $202.5 \mu\text{H}$ and L_2 being $204.4 \mu\text{H}$ and the coupling coefficient between the two mutually coupled coils is 0.11. The resistance R_1 and R_2 are 0.258Ω and 0.288Ω , respectively. The input voltage is the grid voltage and is set with an amplitude of 325 V. The battery profile used for analysis has a battery voltage varying from 290 to 400 V, with a maximum battery current of 8.5 A. The compensation network chosen here is a series-series compensation network and the mathematical modelling for the complete network is as follows.

The DC load resistance, R_L can be expressed as an AC equivalent resistance as

$$R_L = \frac{\pi^2}{8} \cdot R_{ac} \quad (4.1)$$

According to [26], the output current in terms of input voltage as

$$I_{out} = \frac{2}{\pi} \cdot \frac{V_{AB}}{j\omega M} \quad (4.2)$$

The output power is the product of output voltage and output current:

$$\begin{aligned} P_{out} &= V_{out} \cdot I_{out} \\ &= \frac{2}{\pi} \cdot \frac{V_{AB} V_{out}}{\omega k \sqrt{L_1 L_2}} \end{aligned} \quad (4.3)$$

where V_{AB} is the peak of the fundamental component of the voltage obtained at the H-bridge converter output port.

From the output point of view, an EV battery charging profile has two phases of operation. The first is called constant current (CC) mode wherein the battery voltage increase gradually and so does the state of charge of battery. The second phase is called constant voltage (CV) mode, where once the peak voltage of the battery is attained, thereby peak power. At this point, the battery has reached most of the charge, and the current is gradually reduced while keeping the voltage constant.

During the CC phase, the output current stays constant. Thus, from (4.2), considering the mutual coupling coefficient is kept constant, we can infer that the input voltage remains constant throughout the operation even though the output voltage is varied from its minimum to maximum level. The input voltage is supplied by the grid and hence the amplitude of grid current is fixed at $230\sqrt{2}$ V at an operating frequency of 50 Hz. The battery voltage varies from 290 V to 400 V and it's expected peak power is 3.5 kW. The output power can be obtained from the product of output voltage and current as both the parameters are known, and its worthy to note that the current stays constant at 8.5 A (its peak amplitude) during the CC mode while the voltage is kept varying from its minimum to the maximum level.

Figure 4.9 shows that the output voltage of the matrix converter actually is a 50 Hz waveform with each of its half pulse possessing a waveform varying in terms of the 85 kHz switching frequency. So for a half period of 10 ms, it can be seen from Figure 4.9, the curve operates at the set switching cycle. So the output voltage of the matrix converter can be expressed as the time integral of its amplitude and sinusoidal variation with respect to its angular frequency:

$$\begin{aligned} V_{AB} &= \frac{4}{\pi} \cdot \int_0^{2\pi ft} V_m \sin \omega t \, d\omega t \\ &= \frac{4}{\pi} \cdot \frac{V_m}{2\pi ft} \cdot [-(-1) + 1] \\ &= \frac{4}{\pi} \cdot \frac{V_{in} \sqrt{2}}{0.01\pi 50} \end{aligned} \quad (4.4)$$

Incorporating (4.4) in (4.3) provides the delivered output power to the battery load which, for the same coupling factor, it depends on the output voltage. From (4.3), it is clear that the output voltage could be regulated to control the amount of transferred power to the output. This could be done with a DC/DC converter.

4.3. Simulation of WPT model using DD coil

The system shown in Figure 4.10 has been simulated by using LTSpice as a circuit simulator.

Table 4.1: DD coil parameters

Parameter	Value
Primary inductance	202.5 μ H
Secondary inductance	204.4 μ H
Coupling coefficient	0.11
Primary resistance	0.258 Ω
Secondary resistance	0.288 Ω

4.3.1. Analysis

The DD coil (that's available in the lab) parameters are summarized in Table 4.1.

The battery parameters used for the analysis are summarized in Table 4.2.

Table 4.2: Battery parameters

Parameter	Value
Minimum battery voltage	290 V
Maximum battery voltage	400 V
Maximum output current	8.5 A
Maximum output power	3500 W
Input grid power	3700 W

The capacitance of the series-series compensation network can be calculated using $C = \frac{1}{L \cdot \omega_{res}^2}$, therefore $C_1 = 17.313nF$ and $C_2 = 17.152nF$. Since the grid voltage is constant, the output voltage could be controlled through a DC/DC converter in accordance to target output power according to (4.3). As a result, the output voltage is obtained to be 175.53 V for the enlisted parameters.

4.3.2. Results

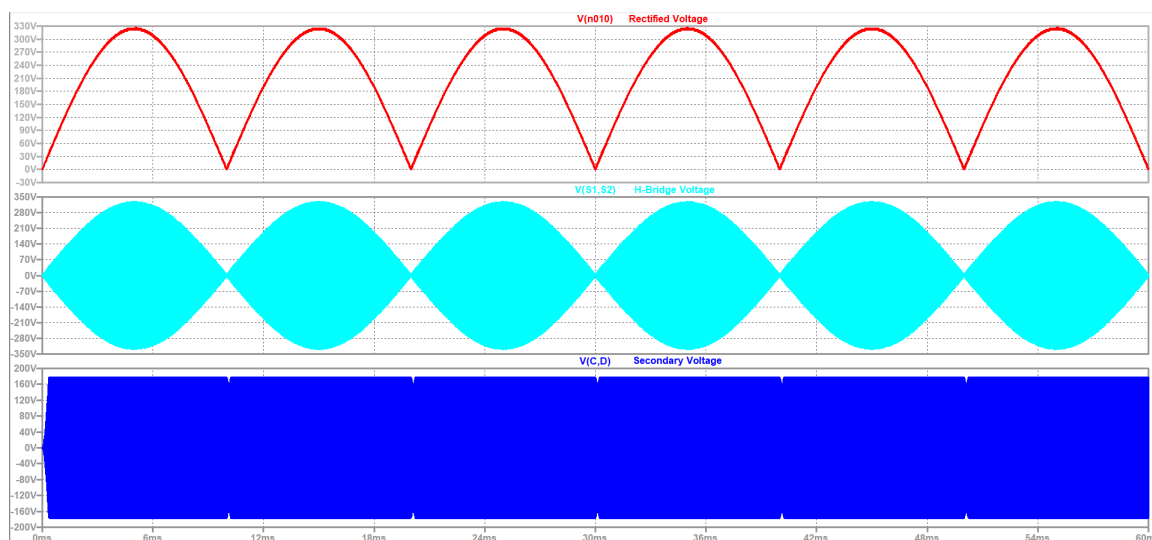


Figure 4.11: Simulation result of single-phase matrix converter voltages. X-axis depicts the time in seconds (sec) and Y-axis depicts the voltage in volt (V).

Figure 4.11 shows the voltages at the rectifier, output of H-bridge converter and in the secondary compensation network. The input grid voltage at 50 Hz is rectified as expected, that is, only the positive pulses are obtained after the rectifier and this rectified voltage is fed to an H-bridge converter operating at 85 kHz. The voltage seen at the output port of the H-bridge is seen to be a 50 Hz sinusoidal curve comprising square waves operating at 85 kHz. In this way, the grid side AC voltage operating at 50 Hz is converted to an AC voltage operating at 85 kHz. The output voltage of the H-bridge converter is fed to the primary compensation network which operates as a resonant tank at the switching frequency of the converter. The high-frequency voltage received at the secondary side is then converted to a DC voltage through the rectifier bridge.

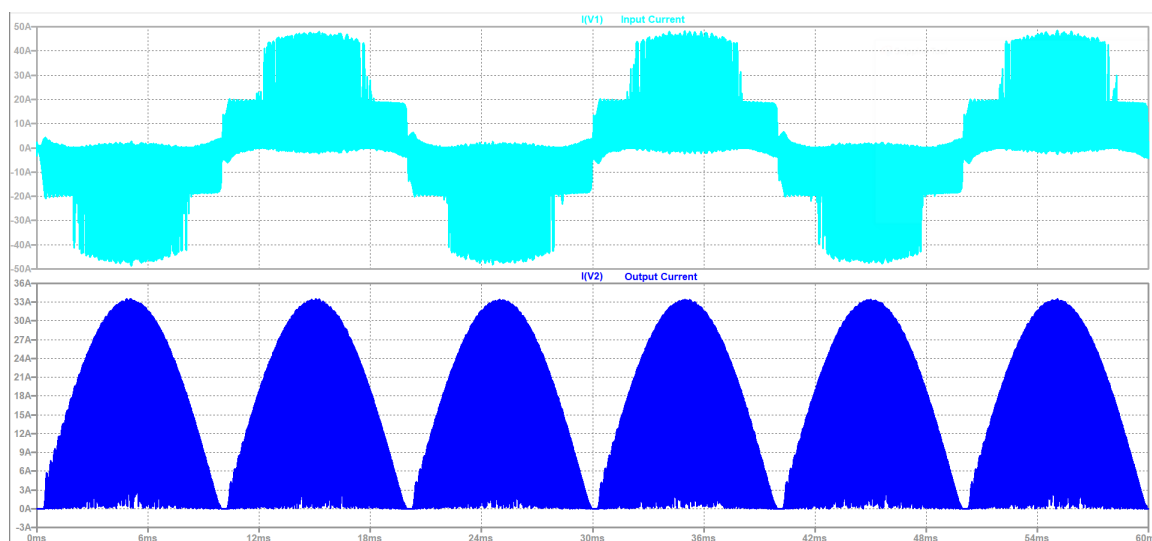


Figure 4.12: Simulation result of single-phase matrix converter currents. X-axis depicts the time in seconds (sec) and Y-axis depicts the current in ampere (A).

The grid current must have a sinusoidal profile and should have its harmonic components within the permissible range given by the IEC 61000-3 standard. In order to mitigate the distortion of the grid current and make it within the permissible range, input filters must be used. Input filters are tuned such that the filter frequency is at least ten times more than the grid frequency and less than one third of the switching frequency. Moreover, the RMS input current must be less than 16 A according to SAE J2954.

Figure 4.12 shows the grid current and the output current. The RMS grid current is well within the permissible range of 16 A, but the waveform has considerable harmonic components.

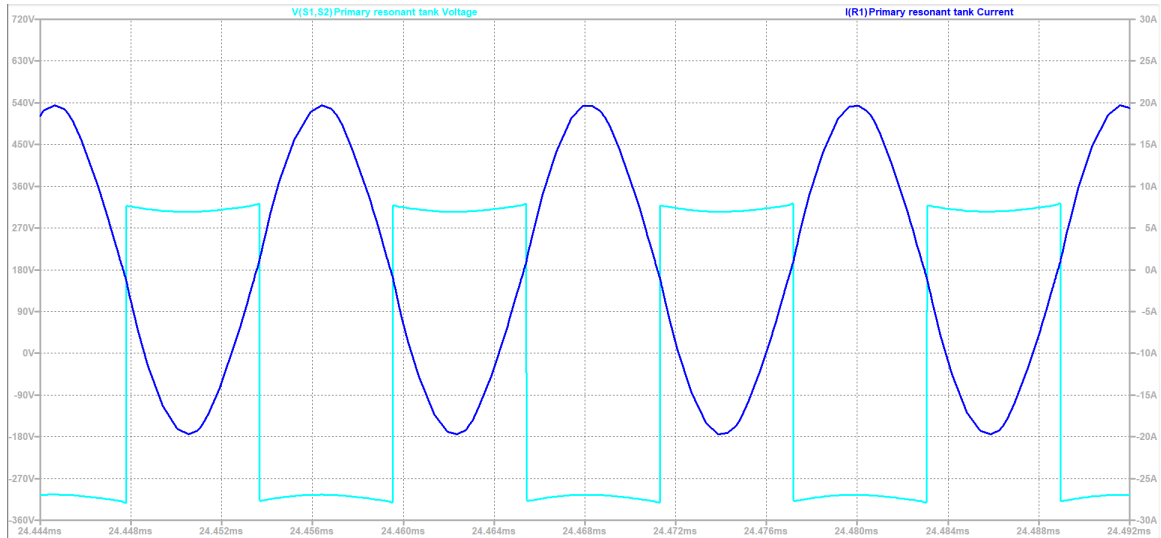


Figure 4.13: Simulation result of Single phase matrix converter - ZVS analysis. X-axis depicts the time in seconds (sec), left Y-axis depicts the voltage (sky blue) in volt (V) and right Y-axis depicts the current (dark blue) in ampere (A).

Figure 4.13 shows that the current across the primary resonant tank is in phase with the resonant tank voltage. The system is operating in zero current switching mode, in case of ZCS, the discharge of internal capacitance of MOSFET during transition is not prominent and hence it is desired to operate the switch in ZVS mode. It is necessary that current lags voltage, for attaining soft switching, which helps reducing the switching losses drastically. In order to make the system more inductive, either the resonant tank frequency can be reduced by increasing the passive component or by varying the switching frequency.

4.4. Zero Voltage Switching (ZVS)

4.4.1. Operating Principle

As seen in Figure 4.13, the inverted voltage from the inverter in Figure 4.10 is a square wave whereas the current resembles a sinusoidal wave. If the inverted voltage crosses the zero when the current is still positive during the transition from the positive to the negative pulse, the conducting switches M5 and M8 turn off and, at this time, the switches M6 and M7, which were blocking the input voltage, would have their internal capacitance charged to the DC supply voltage. In the case that the current is lagging behind voltage, i.e. current is still positive when the inverter switches, the anti-parallel diode across both M5 and M8 would conduct providing the path for capacitor voltage discharge and a path for the positive current to flow. Meanwhile, the switches M6 and M7 are turned on such that once the current reaches zero and becomes

more negative, they naturally start conducting and, hence, the system attains zero voltage switching (ZVS) turn-on, which minimized the inverter's switching losses.

4.4.2. Resonant Tank Tuning

The resonant tank frequency is reduced from 85 kHz in order to attain ZVS turn-on operation of the inverter. In this way, by switching at 85 kHz, the WPT system would operate in the inductive region of the resonant tank which means that the inverter current lags the inverted voltage. Reducing the resonant frequency would increase the value of the compensation capacitance, provided the coil parameters are maintained as suggested in Table 4.1. The capacitance value is increased to 18.5 nF in the primary tank making it misaligned and as well the frequency is stepped down from the center frequency. The system at the resonant frequency must be resistive and at zero phase but in WPT module, since there are two resonant tanks and there could be possibility that there are more than one zero phase condition and this leads to bifurcation. Increasing or going beyond the center frequency, makes the system capacitive and going further far might make the system inductive, rather it is preferred to reduce the resonant frequency and hence the capacitance is made to mismatch.

4.4.3. Bifurcation in WPT systems

Bifurcation is a phenomenon where the phase angle of the transmitter current have multiple zero crossing points, depending on the output load and the magnetic interaction of the coils. Operation above the resonant frequency causes the system to become more capacitive, due to which the switches transition from positive to negative amplitude in hard-switching rather than in soft-switching. In order to ensure soft switching, the system must be more inductive and as well be bifurcation-free. To attain bifurcation-free state for SS compensation, the load resistance be defined well above the limit specified in (5.1).

The stability criterion [27] that must be satisfied by the system to be bifurcation-free for SS compensation network is given by,

$$R_{ac,bifurcation} > \omega_{resonance} L_2 \sqrt{2(1 - \sqrt{1 - k^2})} \quad (4.5)$$

The bifurcation in WPT systems is explained in Chapter 5.

4.4.4. Results

Figure 4.14 shows the behaviour of current and voltage when the resonant tank frequency is reduced by increasing the capacitance. It shows that the current lags the voltage well enough and ensures the fact that the converter is in soft switching mode.

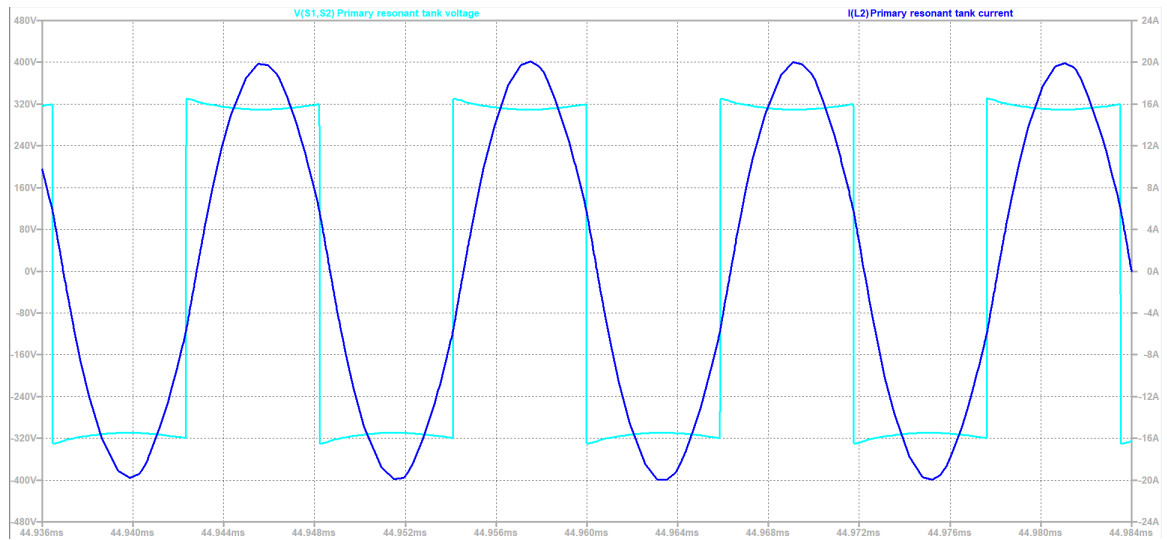


Figure 4.14: Simulation result of Single phase matrix converter - ZVS achieved. X-axis depicts the time in seconds (sec), left Y-axis depicts the voltage (sky blue) in volt (V) and right Y-axis depicts the current (dark blue) in ampere (A).

Table 4.3 shows the maximum permissible RMS current for different harmonic order. Table 4.4 shows the observed Fourier components (Peak current) of the grid current obtained in Figure 4.15. It can be seen that the current value of the seventh harmonic content is not within the standard limit. Filter components must be introduced such that the current amplitude seen in the lower frequency range are well attenuated and at the same time, the higher order harmonics are eliminated completely.

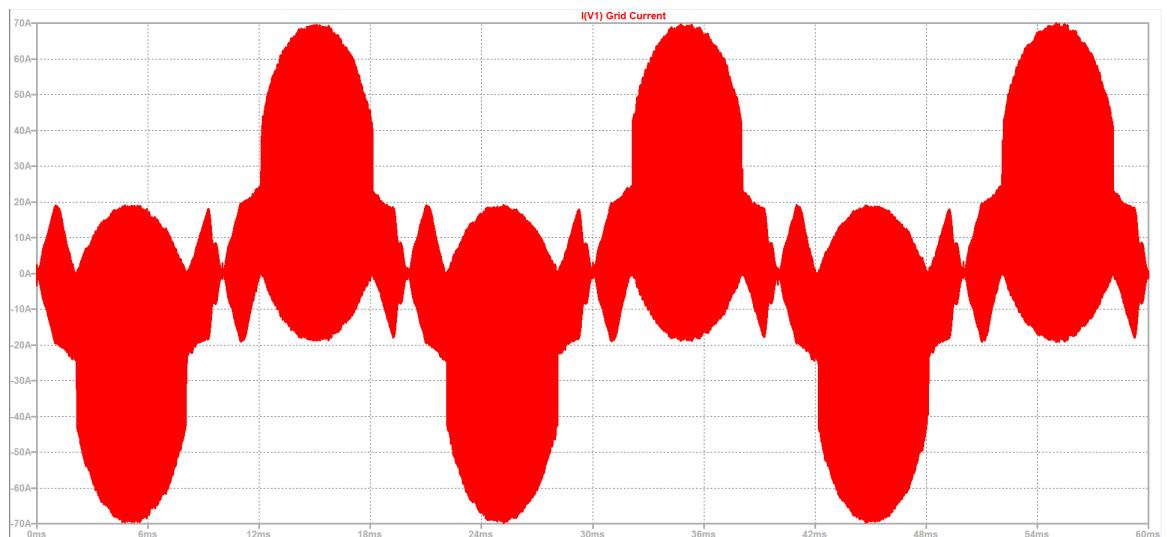


Figure 4.15: Grid current of Single phase matrix converter - ZVS achieved. X-axis depicts the time in seconds (sec) and Y-axis depicts the current in ampere (A).

Table 4.3: Harmonic limits for Class A equipment, as prescribed IEC 61000-3-2.

Harmonic order	Maximum Permissible current (A)
Odd harmonics	
3	2.30
5	1.14
7	0.77
9	0.40
11	0.33
13	0.21
$15 \leq h \leq 39$	$0.15 (15/h)$
Even harmonics	
2	1.08
4	0.43
6	0.30
$8 \leq h \leq 40$	$0.23 (8/h)$

4.5. Input LC Filter

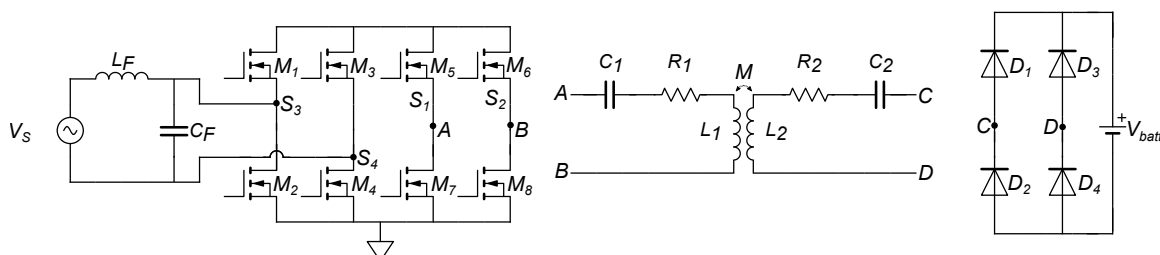


Figure 4.16: Single-phase matrix converter with the resonant tank and battery load with input LC filter.

Figure 4.16 shows an input LC filter connected to the primary converter model just after the grid supply voltage. The input LC filter mitigates the higher order harmonics and reduces the amplitude of lower order harmonics. The cut-off frequency of an ideal LC filter is given by

$$\omega_{fc} = \frac{1}{\sqrt{L_f \cdot C_f}} \quad (4.6)$$

Generally, it is designed to have a cut-off frequency higher than 20 times the grid frequency and three times lower than the switching frequency [28]. One of the passive components (inductor or capacitor) is assumed and the other component is designed based on the chosen cut-off frequency. In this design, the chosen cut-off frequency is 14 kHz and assumed inductance is 40 μH , Based on these parameters, the filter capacitance is calculated to be 3 μF .

The input LC filter circuit used for the reduction of switching noise is shown in Figure 4.17.

Table 4.4: Peak currents obtained for different harmonic order

Harmonic Number	Frequency [Hz]	Fourier Component
1	50	2.08
2	100	3.6e-3
3	150	1.78
4	200	1.3e-2
5	250	1.00
6	300	2.7e-2
7	350	1.39
8	400	1.0e-2
9	450	1.08

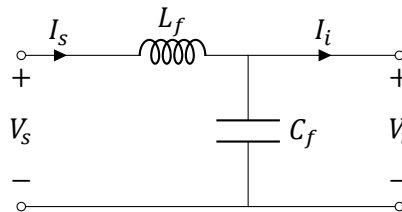


Figure 4.17: Input LC Filter

In the above figure, V_s is the grid supply voltage, I_s is the grid current drawn, I_i is the converter input current, V_i is the converter input voltage, L_f is the filter inductance and C_f is the filter capacitance. Based on the voltage and current equations derived Figure 4.17, the transfer function can be written as:

$$\begin{aligned}
 I_s(s) &= H_V(s)V_s(s) + H_I(s)I_i(s) \\
 H_V(s) &= \frac{sC_f}{s^2L_fC_f + 1} \\
 H_I(s) &= \frac{1}{s^2L_fC_f + 1}
 \end{aligned} \tag{4.7}$$

where $H_V(s)$ is the transfer function related to the grid supply voltage and $H_I(s)$ is the transfer function related to the converter input current [29].

For the selected design parameters, the frequency response for $H_I(s)$ of the input LC filter is shown in Figure 4.18.

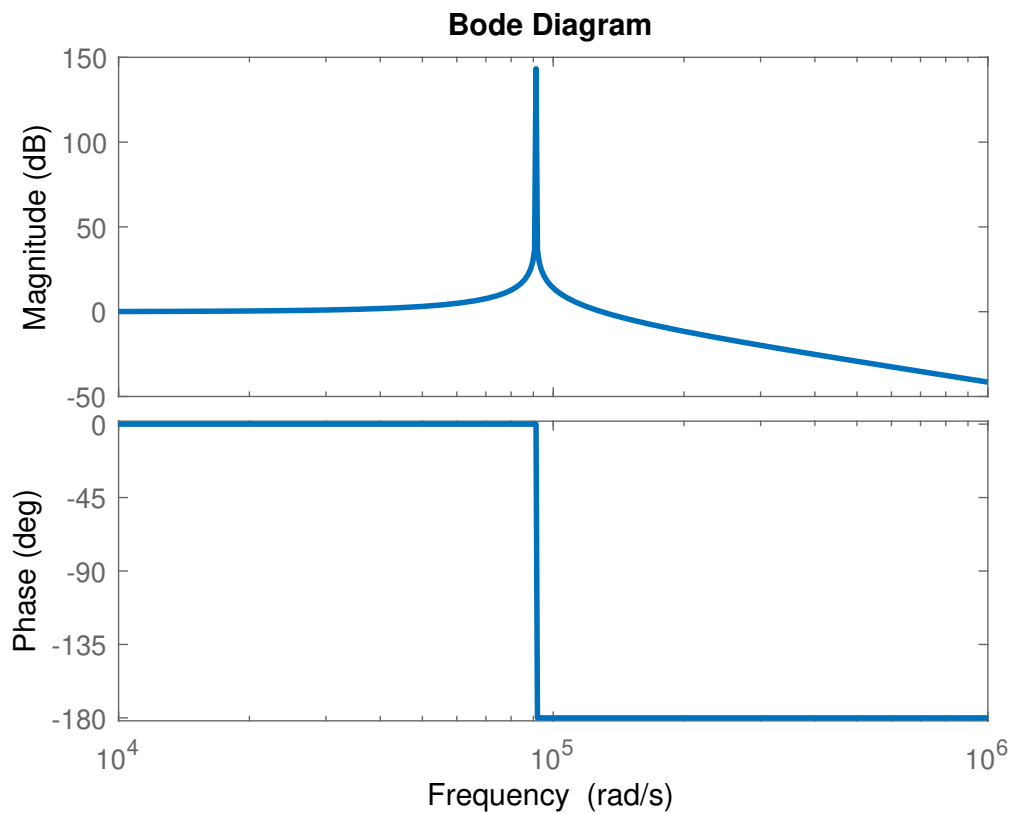


Figure 4.18: Bode Plot LC filter

From Figure 4.18, it can be observed that the gain at the cut-off frequency (around 90,000 rad/s) is high. There is also a rapid phase-change at this point. To avoid such a sharp response in the system, damping resistor is used.

4.5.1. Damped LC Filter

A resistor is added in parallel to the filter inductor of the input LC filter to damp its response. This is implemented as shown in Figure 4.19.

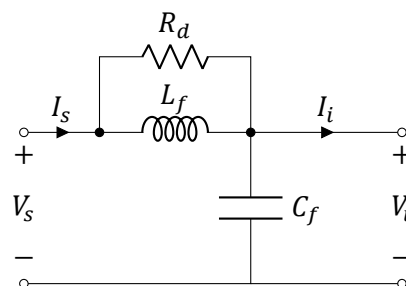


Figure 4.19: Input LC Filter

The resulting transfer function for the damped LC filter can be expressed as:

$$\begin{aligned}
 I_s(s) &= H_{V_d}(s)V_s(s) + H_{I_d}(s)I_i(s) \\
 H_{V_d}(s) &= \frac{sC_f(R_d + sL_f)}{s^2R_dL_fC_f + sL_f + R_d} \\
 H_{I_d}(s) &= \frac{R_d + sL_f}{s^2R_dL_fC_f + sL_f + R_d}
 \end{aligned} \tag{4.8}$$

For the damped LC filter, the cut-off frequency remains the same as (4.6) [28]. The use of the resistor gives rise to a damping factor which is given by:

$$\zeta = \frac{1}{2R_d} \sqrt{\frac{L_f}{C_f}} \tag{4.9}$$

Various damping value for the resistor can be considered to optimise the frequency response of the filter as shown in Table 4.5.

Table 4.5: Peak currents obtained for different harmonic order

Serial Number	Damping Resistance (Ω)	Damping Ratio (ζ)
1	0.001	1825.74
2	1	1.83
3	3	0.61
4	10	0.18
5	100	0.02

Based on this variation, the frequency response is plotted in Figure 4.20. Based on the figure, it can be observed that for low damping ratios, the gain increases exponentially. For higher damping, the gain reduces, thus leading to a more stable system. The high damping however can lead to increased power losses in the damping resistor and thus, its design must be optimised considering the response and the power losses. Based on this consideration, a damping resistance of 3 Ω is chosen for this design.

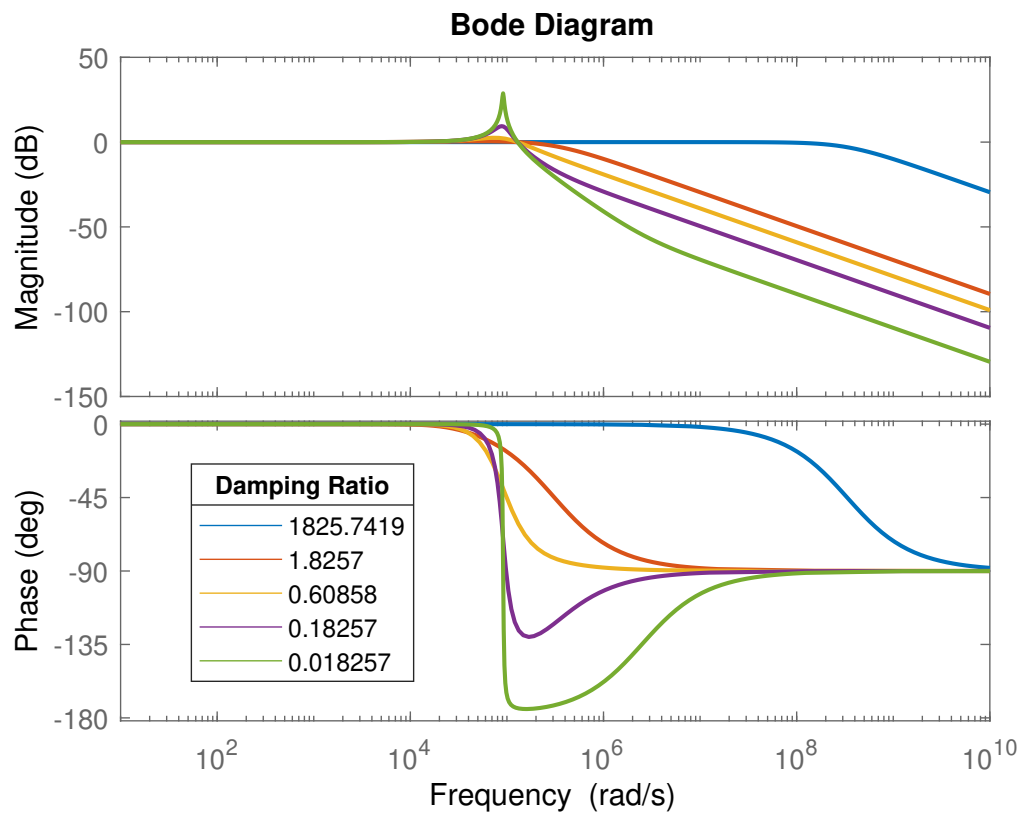


Figure 4.20: Bode Plot LC filter with damping

4.6. Effect of input filter on inductor current

4.6.1. Ideal LC filter

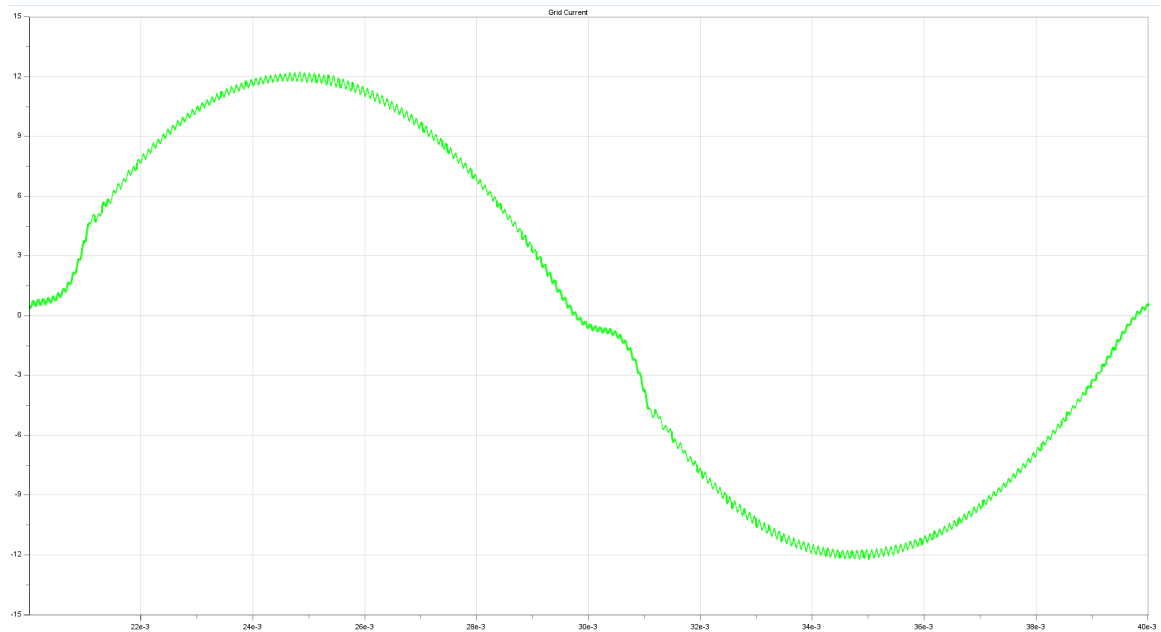


Figure 4.21: Effect of LC filter on grid current. X-axis depicts the time in seconds (sec) and Y-axis depicts the current in ampere (A).

4.6.2. Damped LC filter

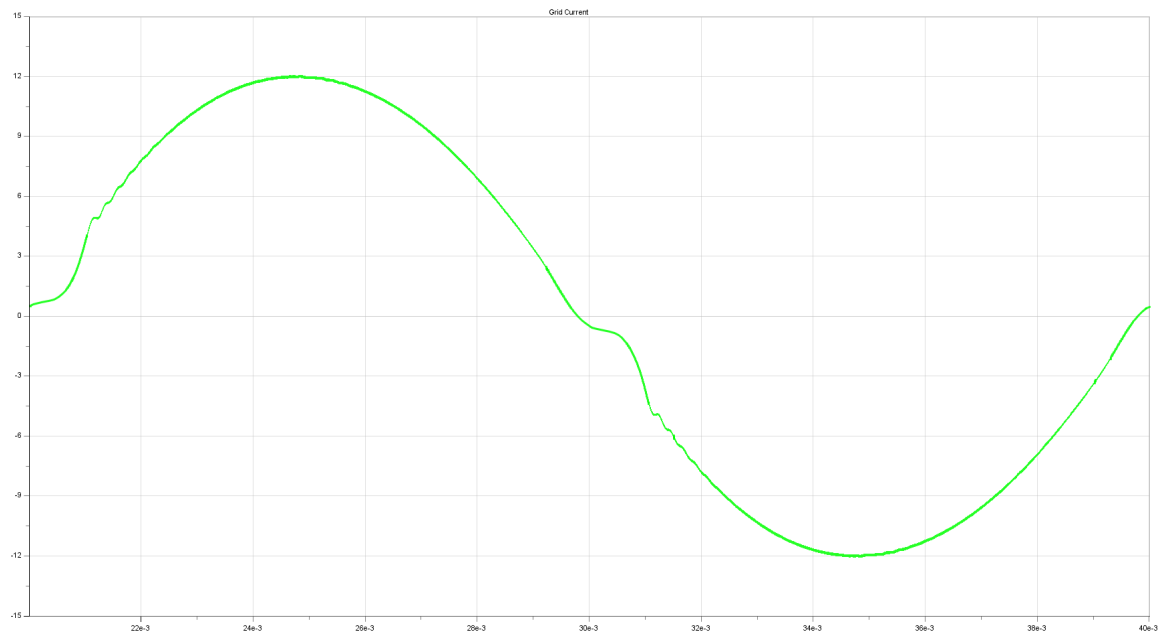


Figure 4.22: Effect of Damped LC filter on grid current. X-axis depicts the time in seconds (sec) and Y-axis depicts the current in ampere (A).

Figure 4.21 shows the effect of ideal LC filter on the grid current. In comparison with Figure 4.15, the ideal LC filter has attenuated the high frequency components, making it more sinu-

soidal. Table A.1 shows the FFT for the first 40 harmonics. The fourier components are well within the prescribed limits.

Figure 4.22 shows the effect of damped LC filter on the grid current. In comparison with Figure 4.21, the damped LC filter has much less pulsations and Table A.2 shows the improvement in the fourier components.

5

Three Phase Matrix Converter

This chapter deals with the analysis of three-phase matrix converter for WPT applications. This chapter starts with a description of the structure of the three-phase matrix converter, followed by the formulation of gating pulses as to attain soft switching. The converter losses were determined for the complete system and the approximate system efficiency was calculated. The effect of load variation on the system was examined. Finally, the input current control was implemented to reduce the higher order harmonics.

5.1. Implementation

The three-phase matrix converter is an extension of single-phase matrix converter. The three-phase topology analyzed in this research is shown in Figure 5.1. This system is a three-wire system with a common neutral point. The three negative potentials are star-connected, where the common point acts as the neutral, and the positive polarity is fed to the input filter [24]. Each single-phase module possesses a rectifier bridge which converts the grid AC voltage operating at 50 Hz to a repetitive positive half-wave. This positive half-wave is fed to the H-bridge switching at a frequency of 85 kHz. The output voltage from each H-bridge is fed to a highly coupled transformer, whose secondary windings are connected in series as shown in Figure 5.1. Since the turns ratio is 1:1, the voltage seen at the primary is ideally transferred to the secondary. The voltage from the three terminals gets simply added up. Each phase voltage of the three-phase grid is shifted by a phase angle of 120 degrees, and hence, the output voltage of the series connected transformer would be a step voltage added up based on the phase difference. The step voltage can be symmetrical or asymmetrical based on the gating pulse generated. The generated voltage is fed to the primary resonant tank which is mutually coupled to the secondary resonant tank and the battery load.

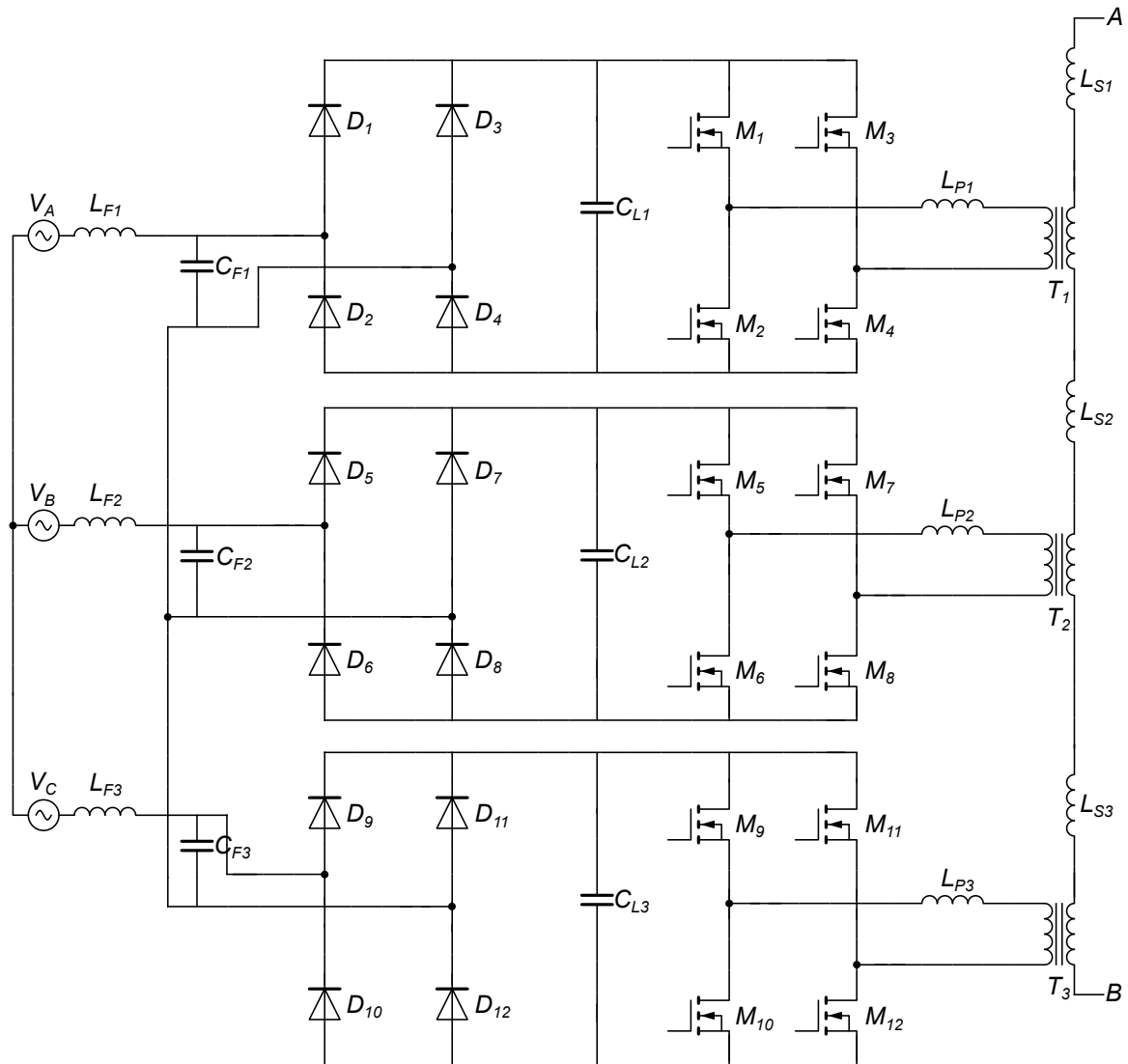


Figure 5.1: Proposed three-phase matrix converter implementation.

5.2. Three-phase matrix converter for WPT application

The three-phase matrix converter is a primary converter used to convert the grid AC voltage to a high frequency AC voltage. The high frequency current in the primary side coil, transmitting coil, induces an AC voltage at the secondary side which is then rectified to obtain a DC voltage. The three-phase matrix converter is initially analysed with DD coils-based resonant tank and its effects on the system is listed. Effect of changing the coil (from DD coil to rectangular coil, in order to increase the mutual inductance) is analysed and explained.

5.2.1. DD coil based resonant tank

The series-series resonant tank is added to the three phase matrix converter model shown in Figure 5.1. A and B terminals of the secondary transformer is connected to the series-series resonant tank terminals. The secondary side of the resonant tank is connected to the rectifier which is then connected to the battery load. The resonant tanks is parameterised as discussed in the previous chapter. The coupling factor is retained to be at 0.11. In order to maintain the soft switching of the converter, the resonant tank frequency is slightly reduced, reducing the resonant tank frequency increases the capacitor value considering the coil to be

fixed. The H-bridge MOSFETs are controlled through asymmetric pulse disposition as shown in Figure 5.2(e) in order to achieve ZVS in all the three phases. The reference wave is compared with sawtooth waveform phase shifted at 180° . The rectifier bridge output is sinusoidal waveform voltage due to the presence of small capacitance. The phase shift between the sawtooth waveform, ensures the effect of two sinusoids cancel out each other. When using the symmetric pulse modulation, ZVS is not seen in two phases of the three phases making it ineffective. The carrier wave is offset at its mid range of 500 milli of the maximum amplitude and the triangular pulse is made to have a delay of 1 and it can be noted that instead of usual upper ramp and lower ramp, this generates just the positive ramp and drops directly to zero from the maximum amplitude. The two carrier signals are shifted by 180 degrees. The sinusoidal signal is set at an amplitude of 0.499 and is shifted by 120 degrees for each of the phase. This ensures the asymmetrical generation of pulse and the pulse generated by two adjacent switches are complementary to one another.

Figure 5.3 shows the primary voltage and current, all the three phases validates the fact that system is in ZVS operation. The current lags the voltage, making the system inductive, the current still stays positive even when the voltage transitions from zero to negative. This ensures the accomplishment of soft switching. Figure 5.4 shows the effect of using the highly-coupled transformers. The primary voltage is an unsymmetrical voltage which gets effected in the secondary voltage, the addition of three of the primary voltage effects in the secondary voltage. Figure 5.5 shows that the system is operating at an output power of 17.8 kW, but the EV application we are addressing to is around 3.5 kW. Therefore, for the target power level, (4.3) shows that this topology is suitable for coupled coils with higher mutual inductance M . For this reason, instead of DD coils, a pair of rectangular coils with higher magnetic coupling is used in order to ensure lower output power.

5.2.2. Rectangle coil based resonant tank

The rectangular coil parameters are as follows: The capacitance of the series-series compen-

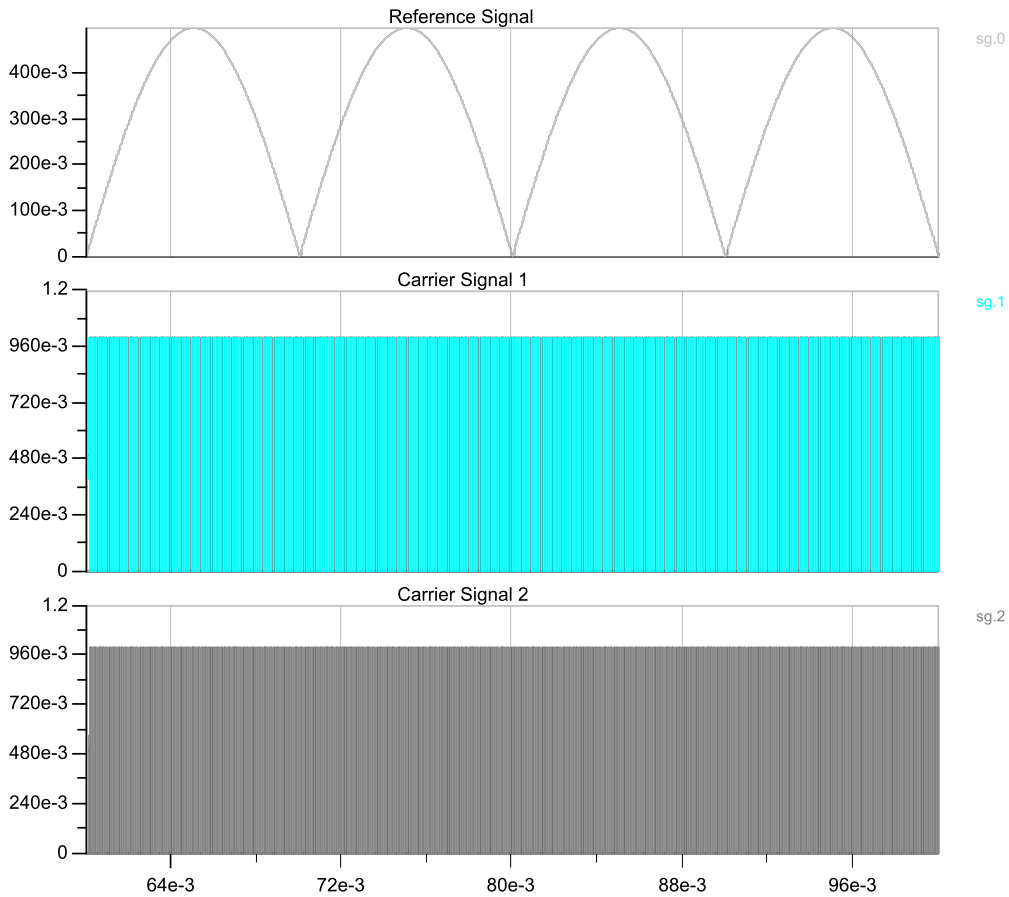
Table 5.1: Rectangular coil parameters

Parameter	Value
Primary inductance	340 μH
Secondary inductance	224.7 μH
Coupling coefficient	0.325
Primary resistance	0.695 Ω
Secondary resistance	0.497 Ω

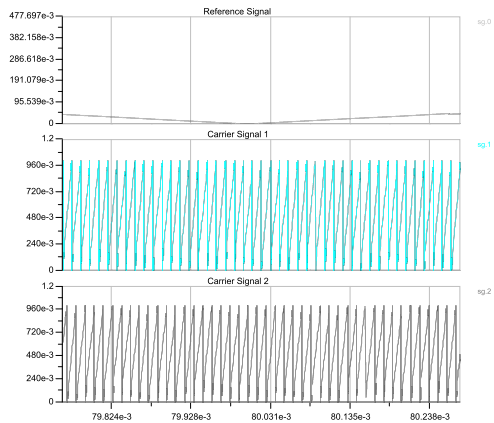
sation network can be calculated by using $C = \frac{1}{L \cdot \omega_{res}^2}$, therefore $C_1=10.31$ nF and $C_2=15.60$ nF. In order to attain soft switching, the primary resonant tank is slightly increased from 10.31 nF to 11.6 nF, ensuring the operation in the inductive region of the resonant tank.

The system must be free from bifurcation process. Substituting (4.1) in (4.5) gives the load resistance to be,

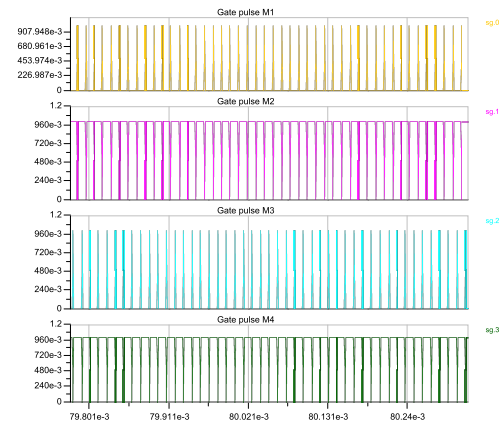
$$R_L > \frac{\omega_{resonance} L_2 \sqrt{2(1 - \sqrt{1 - k^2})} \cdot \pi^2}{8} \quad (5.1)$$



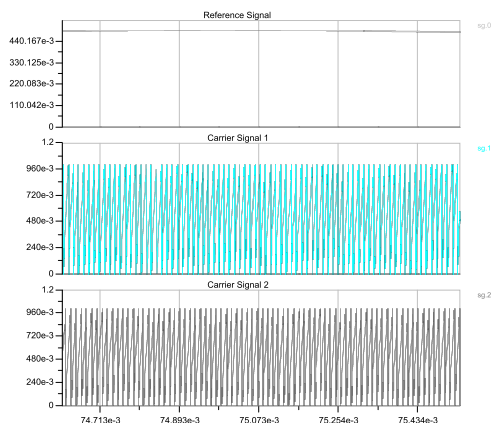
(a) Overview



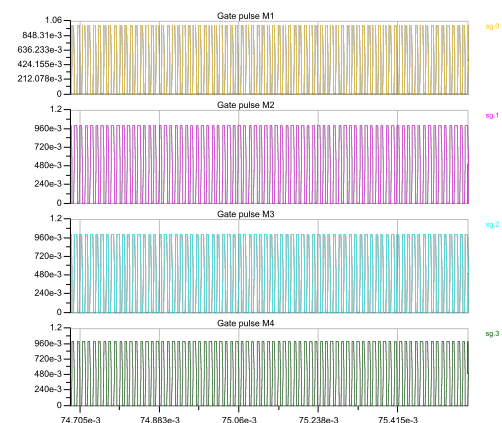
(b) Carrier signal during the transition of reference wave.



(c) Gating signal during the transition of reference wave.



(d) Carrier signal at the peak of reference wave.



(e) Gating signal at the peak of reference wave.

Figure 5.2: Gating pulses for three-phase configuration of the matrix converter. X-axis depicts the time in seconds (sec) and Y-axis depicts the voltage in volt (V).

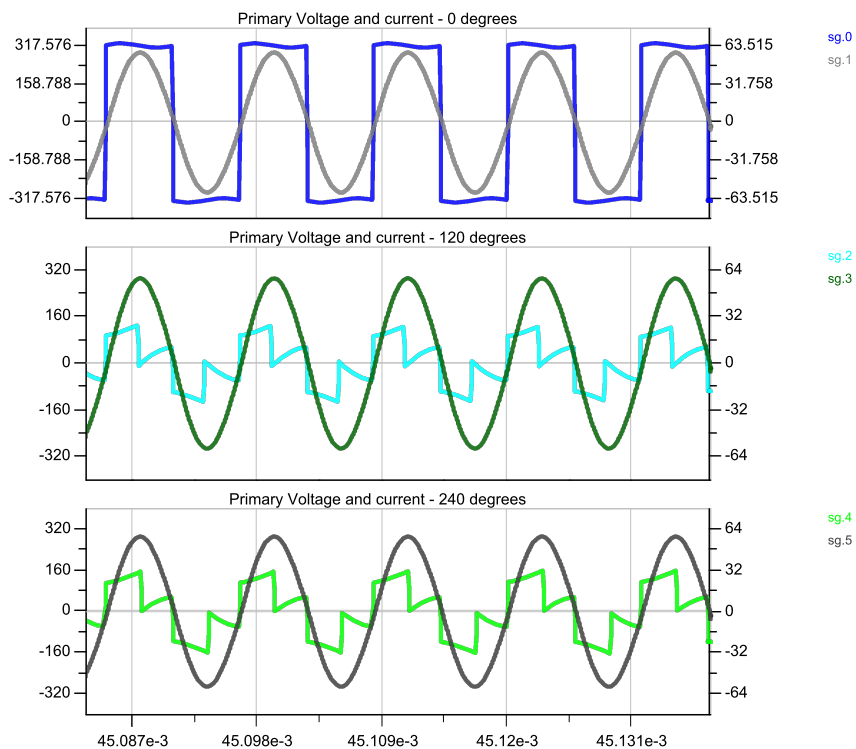


Figure 5.3: Primary transformer voltage and current - DD Coil. X-axis depicts the time in seconds (sec), left Y-axis depicts the voltage (sky blue) in volt (V) and right Y-axis depicts the current (dark blue) in ampere (A).

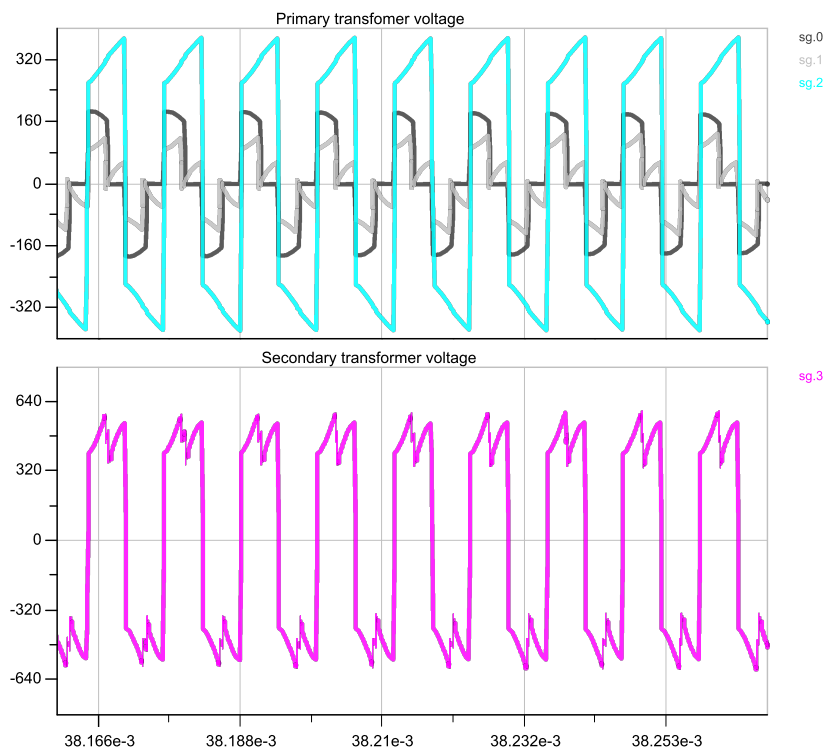


Figure 5.4: Primary and secondary transformer voltage - DD Coil. X-axis depicts the time in seconds (sec) and Y-axis depicts the voltage in volt (V).

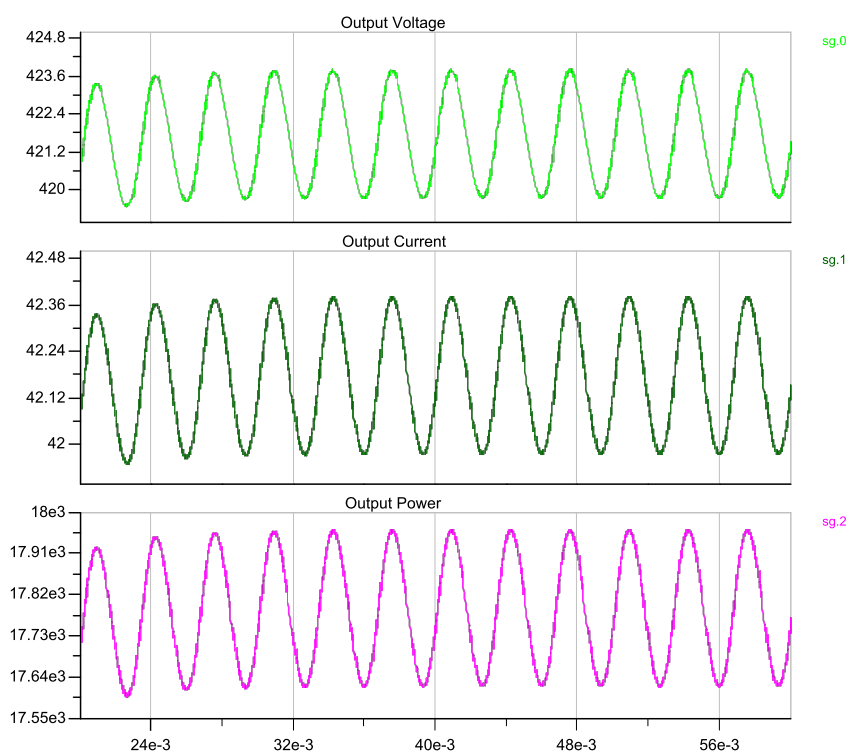


Figure 5.5: Output power of three phase matrix converter - DD Coil. X-axis depicts the time in seconds (sec) and Y-axis depicts the voltage in volt (V) in subplot 1, current in ampere (A) in subplot 2 and power in watts (W) in subplot 3.

Substituting the values of $L_2 = 224.7\mu H$, $k = 0.325$ and resonant frequency to be 85 kHz in (5.1), we obtain $R_L > 48.7832\Omega$. Hence the load resistance is set at 50Ω . Figure 5.6 shows the behaviour of primary voltage and current. Varying the capacitance in the resonant tank, reducing the resonant tank frequency, ensures that the primary current lags behind the primary voltage. The lagging property of current with voltage ensures the zero voltage transition of switching and thereby soft switching operation. This ensures the reduction in switching losses.

Figure 5.7 shows the output voltage and current and as well confirms the fact that the output power has reduced drastically in case of rectangular coil in par to the DD coil. The output power is obtained around the desired value of 3.4 kW.

To confirm if the harmonics of the grid side current in Figure 5.7 are well within the limits set by the IEC 61000-3-2 standard, the FFT was performed. Table A.3 shows the fourier constants obtained for the grid currents which are well within the prescribed limit.

5.3. Evaluation of converter losses and system efficiency

5.3.1. Choice of the switching device

Silicon Carbide (SiC) MOSFETs are preferred over IGBTs and Silicon (Si) MOSFETs.

MOSFETs are preferred over IGBTs as

- IGBT has longer tailing current, and thereby longer switching off time [30].
- On the whole, MOSFETs have lower switching losses, thus can be operated at high

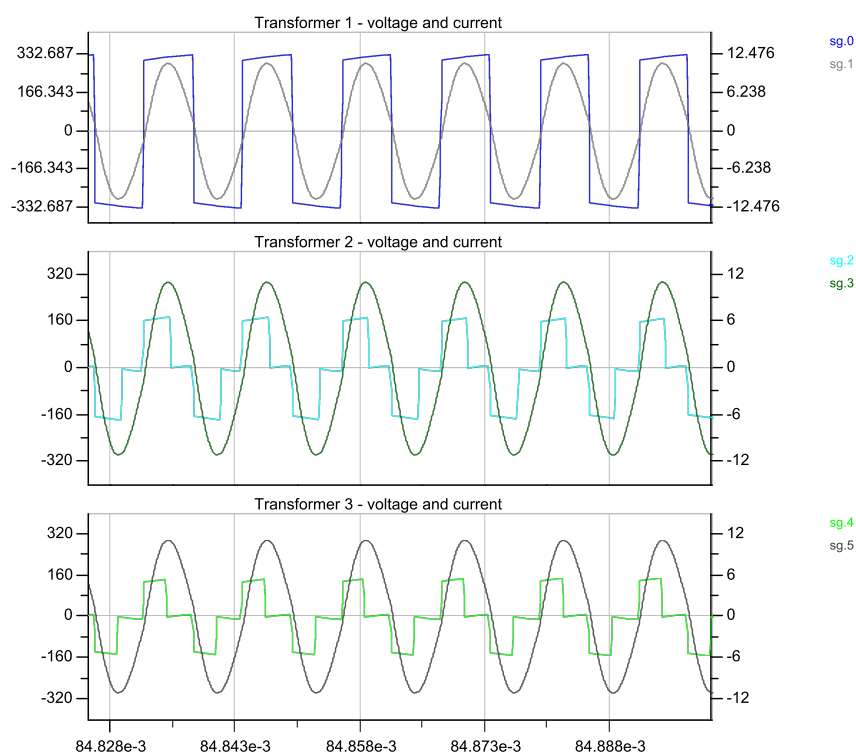


Figure 5.6: Three-phase matrix converter primary transformer voltage and current - rectangular coils. X-axis depicts the time in second (sec), left Y-axis depicts the voltage (square like wave) in volt (V) and right Y-axis depicts the current (sine wave) in ampere (A).

frequencies and they can perform fast switching with low turn-off losses. IGBTs, on the other hand, is a good choice for low frequency operation and losses are relatively high at high frequency operations [30].

- IGBTs are optimum for low frequency, high current operation but not for high frequency and high voltage applications [30].

In terms of MOSFETs, either Si based semiconductors or a silicon carbide (SiC) can be chosen. SiC MOSFETs are chosen [31] as

- The switching losses that is the transition from blocking to conducting mode or vice versa, is lower in case of SiC than Si material.
- When the circuit operates at a higher switching frequency, the passive component volume reduces to achieve the same performance.
- Operates at higher temperature and hence simplified cooling mechanisms.
- SiC MOSFETs can operate at higher voltage rating, while Si-based MOSFETs are preferred for lower voltage rating applications.

Hence, for what concerns the matrix converter, the rectifier bridge and the H-bridge converter are designed using SiC MOSFETs, while the secondary side diode bridge rectifier is designed using SiC Schottky diodes. Though in simulation, diodes were used for rectifier bridge, but in reality, MOSFETs would be used for synchronous rectification. C3M0120090J SiC MOSFET is the switch used for designing the matrix converter. As listed in the datasheet [32], this

MOSFET has high blocking voltage with low on-resistance which determines the conduction loss, high switching speeds, and fast intrinsic diode with low reverse recovery. C5D50065D SiC Schottky diode is the chosen diode for the diode bridge rectifier at the receiver side. The features of this diode as listed in the datasheet [33], zero reverse-recovery current and zero forward recovery voltage ensuring zero switching loss, high frequency operation, extremely fast switching and higher efficiency.

5.3.2. Semiconductor losses

Semiconductor losses comprises of conduction losses and switching losses. Conduction losses occur during the high state of the switch, that is during the on-time of the switch. In the case of a MOSFET, the conduction losses depend on the on-resistance and the drain current. On the other hand, in the case of a diode, the conduction losses depend on the forward volt-

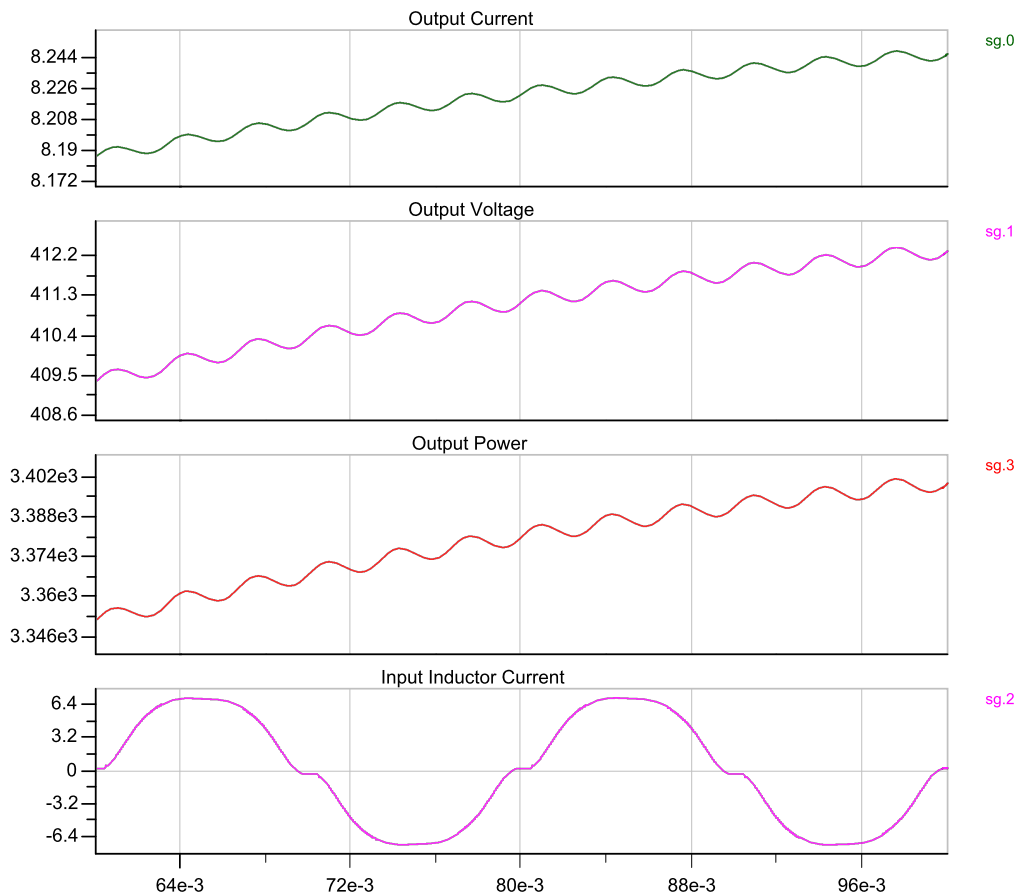


Figure 5.7: Three-phase matrix converter output power and input grid current - rectangular coils. X-axis depicts the time in seconds (sec) and Y-axis depicts the current in ampere (A) in subplot 1, voltage in volt (V) in subplot 2, power in watts (W) in subplot 3 and current in ampere (A) in subplot 4.

age, the current and on the equivalent resistance. Switching losses are the power loss that is consumed during the transition from either blocking mode to conducting mode (turn-on) or from conducting to blocking mode (turn-off). Switching losses depends on the energy loss and the frequency at which the switch operates.

The conduction loss of a MOSFET is given by

$$P_{Conduction} = R_{DS,ON} \cdot I_{D,RMS}^2 \quad (5.2)$$

Considering that the H-bridge is operating in ZVS turn-on, the switching loss of a MOSFET is given by

$$P_{Switching} = E_{off} \cdot f_{switching} \quad (5.3)$$

The conduction loss of a diode is given by

$$P_{Conduction} = V_F \cdot I_{F,av} + R_D \cdot I_{F,RMS}^2 \quad (5.4)$$

- **Matrix converter - Rectifier bridge**

The RMS drain current, $I_{D,RMS}$ of switch pair D1 and D4 is 4.19 A (extracted from simulation) and that of switch pair D2 and D3 is 4.19 A. The drain source on-resistance is deduced from the datasheet. The graph depicts junction temperature versus on-resistance in per unit as shown in Figure A.1. At 125 ° C, the on resistance is approximately 144 mΩ.

Using (5.2), $P_{Conduction}$ for switch D1 and D4 is given as $144 \cdot 10^{-3} \cdot 4.19 \cdot 4.19 = 2.53$ W; and that of switch D2 and D3 is $144 \cdot 10^{-3} \cdot 4.19 \cdot 4.19 = 2.53$ W. The calculated loss is for one switch and as well one phase. So, total conduction loss in one phase summation of twice the calculated losses, which is $2 \cdot 2.53 + 2 \cdot 2.53 = 10.12$ W. Total conduction loss is $3 \cdot 10.12 = \mathbf{30.36$ W.

The synchronous rectifier operates at 50% duty cycle in phase with the grid supply voltage. This ensures ZVS turn and turn off. Thus, the switching losses of the rectifier bridge is **0 W**.

- **Matrix converter - H-bridge**

The RMS drain current, $I_{D,RMS}$ of switch pair M1 and M3 is 4.42 A (extracted from simulation) and that of switch pair M2 and M4 is 6.42 A.

Using (5.2), $P_{Conduction}$ for switch M1 and M3 is given as $144 \cdot 10^{-3} \cdot 4.42 \cdot 4.42 = 2.81$ W; and that of switch M2 and M4 is $144 \cdot 10^{-3} \cdot 6.42 \cdot 6.42 = 5.94$ W. The calculated loss is for one switch and as well one phase. So, total conduction loss in one phase summation of twice the calculated losses, which is $2 \cdot 2.81 + 2 \cdot 5.94 = 17.5$ W. Total conduction loss is $3 \cdot 17.5 = \mathbf{52.5$ W.

The off-state switching energy is deduced from the datasheet. The junction temperature versus switching loss graph provides in accurate value of off state energy at the junction temperature of 125 ° C as shown in Figure A.2. The off-state energy deduced from graph was approximately around 8 μJ.

Since the dc-link voltage is a rectified sinusoidal wave. This effects in a low frequency (100 Hz) voltage and current in the MOSFET. The average turn off current was calculated for a period 10 ms and sampled at 20 uniform points over the period. The average turn off current resulted to be 6.2025 A and average voltage resulted to be 127.2149 V.

For a current of 6.2025, off state energy was found to be 7.5 μJ at 400 V as seen in Figure A.3. The turn off energy was scaled down for the average voltage across MOSFET and this resulted at 2.3852 μJ. For the worst operating temperature of 125 ° C, the obtained energy was multiplied with a factor of 1.2307 (scaling from 25 ° C to 125 ° C) results to be 2.9354 μ J. Using (5.3), the switching loss for a single switch in the H-bridge operating at 85000 Hz is $2.9354 \cdot 10^{-6} \text{ J} \cdot 85000 \text{ Hz} = 0.25$ W. The switching loss of all the four switches in the single phase of the H-bridge is $4 \cdot 0.25 = 1$ W and that for all three phases is triple the amount: **3 W**.

- **WPT receiver - diode rectifier**

The RMS forward current, $I_{D,RMS}$ of switch pair D13 and D16 as shown in A.4 is 6.55 A (extracted from simulation) and that of switch pair D14 and D15 is 6.55 A. The average forward current, $I_{D,av}$ of switch pair 13 and 16 is 4.15 A and that of switch pair 14 and 15 is 4.15 A.

At a junction temperature of 125 ° C, for a RMS current of 50 A and forward voltage of 1.7 V in the linear scale of the graph in datasheet as shown in Figure A.5, the drain resistance can be calculated as 0.03 Ω. So, at a RMS current of 6.55 A and drain resistance of 0.03 Ω, the forward voltage is 0.22 V.

Using (5.2), $P_{Conduction}$ for switch D13 and D16 is given as $0.22 \cdot 4.15 + 0.03 \cdot 6.55^2 = 2.20$ W; and that of switch D14 and D15 is $0.22 \cdot 4.15 + 0.03 \cdot 6.55^2 = 2.20$ W. The calculated loss is for one switch per leg. So, total conduction loss in one phase is summation of twice the calculated losses, which is $2 \cdot 2.20 + 2 \cdot 2.20 = \mathbf{8.80 W}$. The switching losses in the diode is zero as it has zero reverse-recovery current and zero forward recovery voltage.

- **Total semiconductor losses**

The total semiconductor loss is addition of all the losses calculated above, highlighted in bold. The total semiconductor loss is $52.5+3+30.36+8.80 = \mathbf{94.66 W}$.

- **Efficiency**

The input power is found to be 3.53 kW from the simulation and the output power is 3.42 kW. Subtracting the semiconductor losses from the output power, we get the power to 3.32 kW and an efficiency of 94.05%. This is an approximate deduction of efficiency because the simulation considers ideal highly coupled transformers and it does not consider the losses of the input filter.

5.4. Effect on load variation

In the previous analysis, the load was set at 50 Ω for the chosen coupling coefficient of 0.325. For a battery voltage range of 290-400 V and an expected output power of 3500 W, the load resistance ranges from 24.03 to 45.71 Ω. Both the extremes are below the bifurcation value of 48.7832 Ω found in Section 5.2.2. This means that the bifurcation phenomenon would be present during the whole battery charging profile. To achieve the bifurcation-free phenomenon for the whole charging profile, the switching frequency must be set slightly below resonant tank frequency to achieve soft switching.

Lowering the switching frequency to around 83000 Hz ensures zero voltage switching for the load resistance set as it would make the system operate in more inductive region. This ensures zero voltage switching for all the voltage range possible for the battery used.

The equivalent resistive load is lowered to the corresponding minimum voltage rating of the battery profile, and Figure 5.8(a) shows that the system is in inductive mode of operation and hence can very well operate in soft switching and thereby decrease the switching losses of the converter. Likewise, the system is in inductive mode for the equivalent resistance obtained for maximum voltage rating as shown in 5.8(c).

5.5. Converter Control

The whole system acts essentially as a rectifier from input grid supply to the load. For a grid-connected rectifier, we can control two variables:

- The input supply current drawn from the grid. This can be controlled by the converter to ensure it resembles a sinusoidal waveform by mitigation of harmonics. This controller directly controls the grid current based on the set reference point.
- The DC-link voltage at the output. This is to ensure, a constant stable voltage at the output regardless of load variation. This controller generates a current reference for the current controller to act upon and forms the outer control loop.

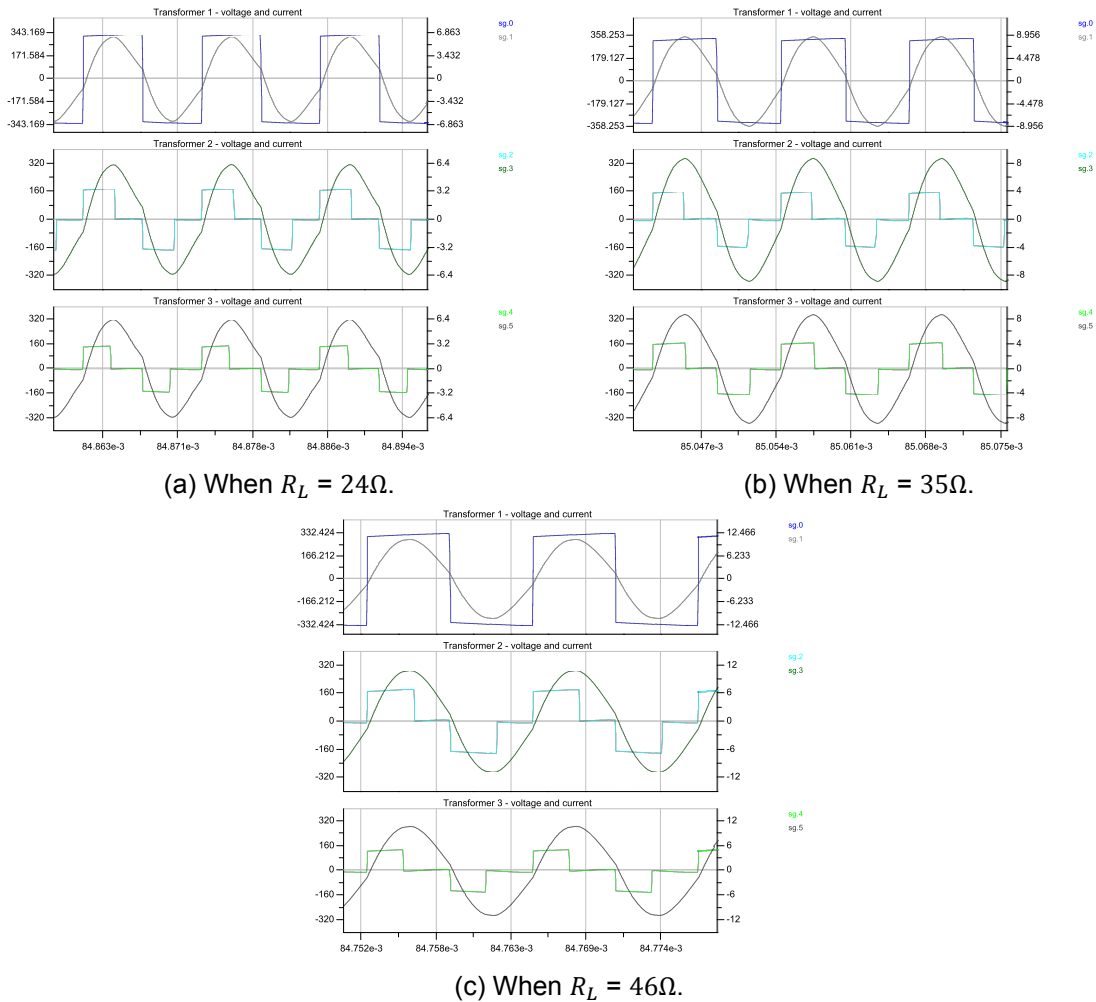


Figure 5.8: Three phase matrix converter transformer primary voltage and current - Load variation. X-axis depicts the time in seconds (sec), left Y-axis depicts the voltage (square like wave) in volt (V) and right Y-axis depicts the current (sine wave) in ampere (A).

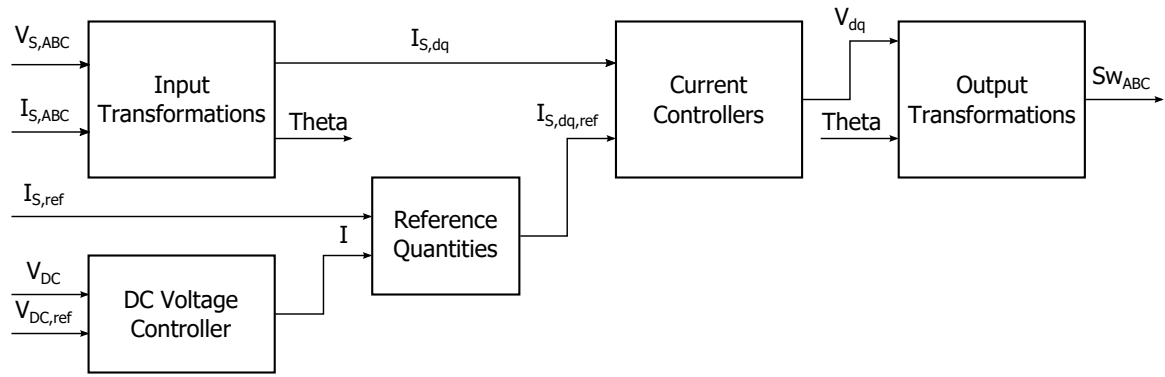


Figure 5.9: Control Scheme

The overall control scheme is presented in Figure 5.9 and is explained in detail below:

- **Input Transformations:** In this stage, the input phase currents in the abc stationary reference frame are transformed into the rotating synchronous reference frame (dq frame). The speed of rotation of this reference frame is determined by the Phase Locked Loop (PLL), which generates an angle reference θ from the grid supply voltage. This will help mitigate the effect of unbalanced grid voltage on the current control.
- **Current Control:** The transformed input currents in the dq frame behave like DC quantities and can thus, be controlled through a Proportional Integral (PI) controller.
- **Voltage Control:** The DC-link voltage is controlled directly through a PI controller, which generates a current reference to be supplied to the current controller.
- **Reference Quantities:** The reference quantities for the current controller are direct set-points in the control of the user. However, the output of the DC-link voltage controller needs to be added to the q-axis current controller to ensure active power transfer to maintain the DC-link voltage.
- **Output Transformations:** In this stage, the converter output voltage from the current controllers in the dq reference frame are converted to the abc reference frame by the use of the PLL-generated reference angle. This voltage is modulated to create the switching pulses for the gate drivers.

5.5.1. Transfer function of converter with LC Filter

The transfer function of a PWM converter is the delay between reference signal input and switching output. For asymmetric sampling, this delay is 0.75 times the switching time-period [34]. This delay can be represented as follows:

$$G_{VSC}(s) = \frac{V_{CD}}{V_{CD,ref}} = e^{-0.75T_s s} \quad (5.5)$$

where T_s is the switching time-period, V_{CD} is the H-bridge output voltage.

The filter transfer function with damping resistor included is given in (4.8). From this equation, we only consider the influence of converter input current and not the grid supply voltage. The input of the matrix converter can be considered as a current source and as a voltage source at the output. Thus, the transfer function with respect to converter input current can directly be used as follows:

$$G_{LC}(s) = \frac{I_s(s)}{I_i(s)} = \frac{R_d + sL_f}{s^2 R_d L_f C_f + sL_f + R_d} \quad (5.6)$$

Thus, the overall open-loop transfer $G_{OL}(s)$ of this system is given by:

$$G_{OL}(s) = G_{VSC}(s) \cdot G_{LC}(s) \quad (5.7)$$

Based on this, the frequency response of $G_{OL}(s)$ is plotted in the form of a Bode plot as shown in Figure 5.10.

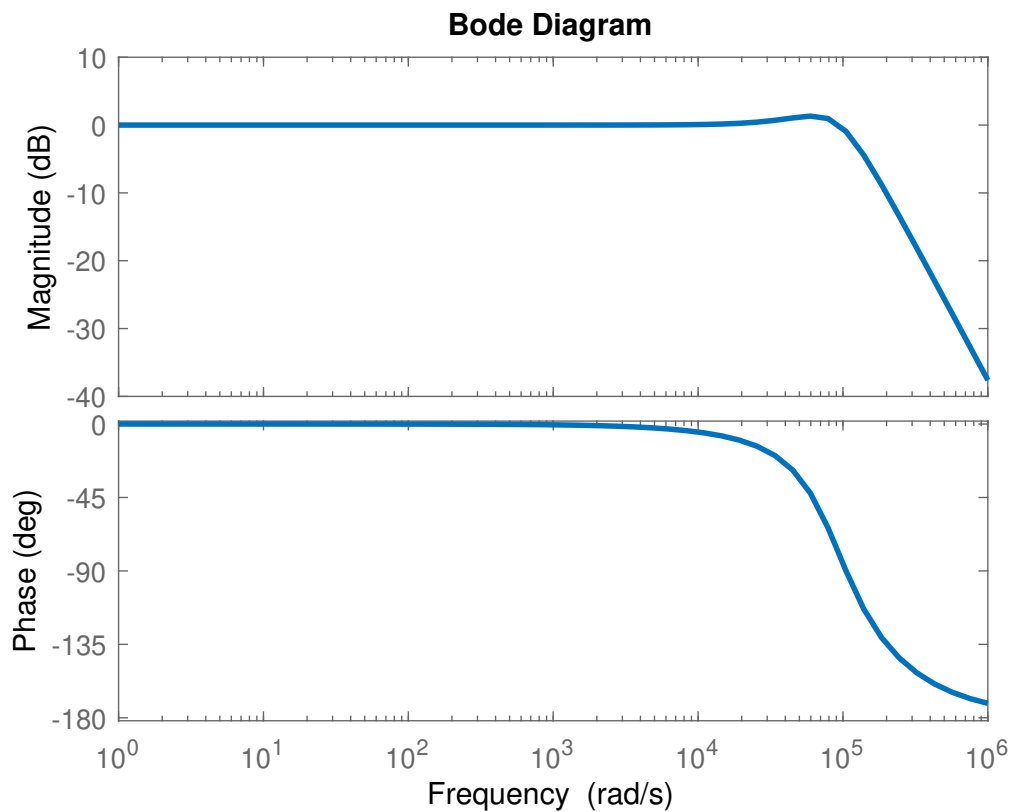


Figure 5.10: Open Loop Frequency Response

According to Figure 5.10, it can be seen that the system is damped well and there is no sudden change in either the magnitude or the phase based on the frequency of operation. It can also be seen that a simple PI controller can help in increasing the gain of the DC component while suppressing the higher order harmonics.

5.6. PI Current Controller

As discussed before, the current controller is designed to control the input current drawn from the grid. This is implemented as a PI Controller in the dq synchronous reference frame as shown in Figure 5.11. Considering this reference frame, the fundamental frequency components of currents to be controlled appear to be DC in the dq frame. Thus, these quantities can be compensated with a PI controller, since these controllers have a high gain at 0 Hz.

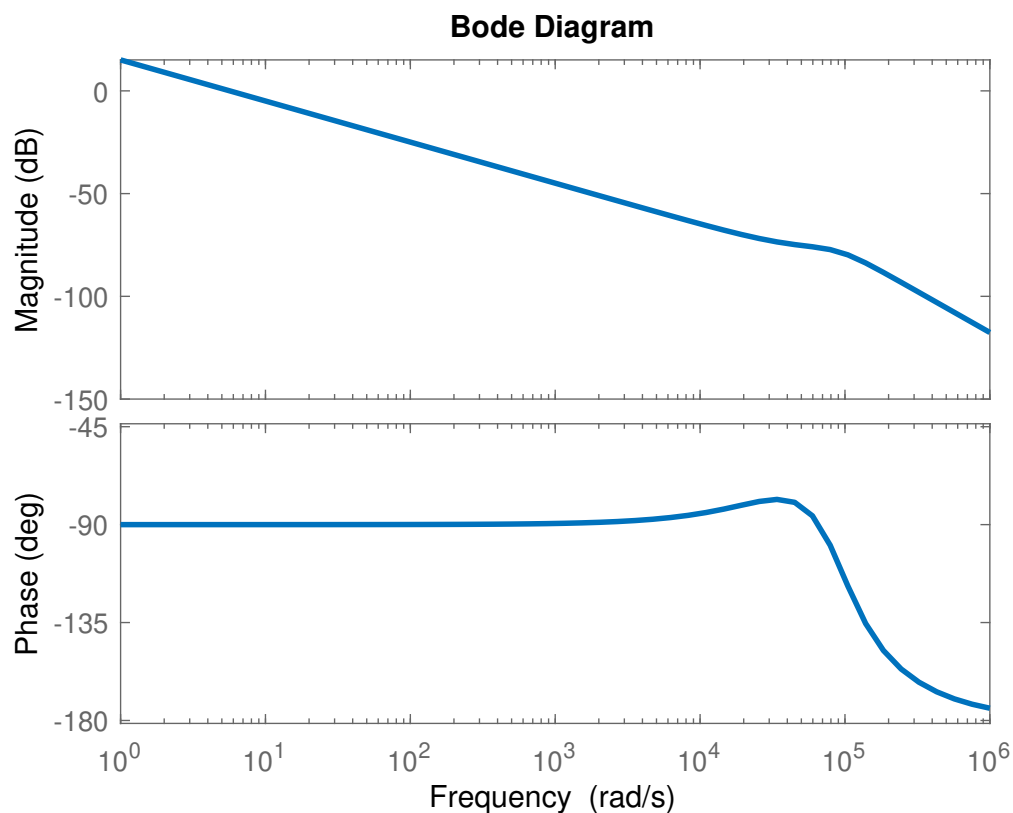


Figure 5.12: Closed Loop Frequency Response

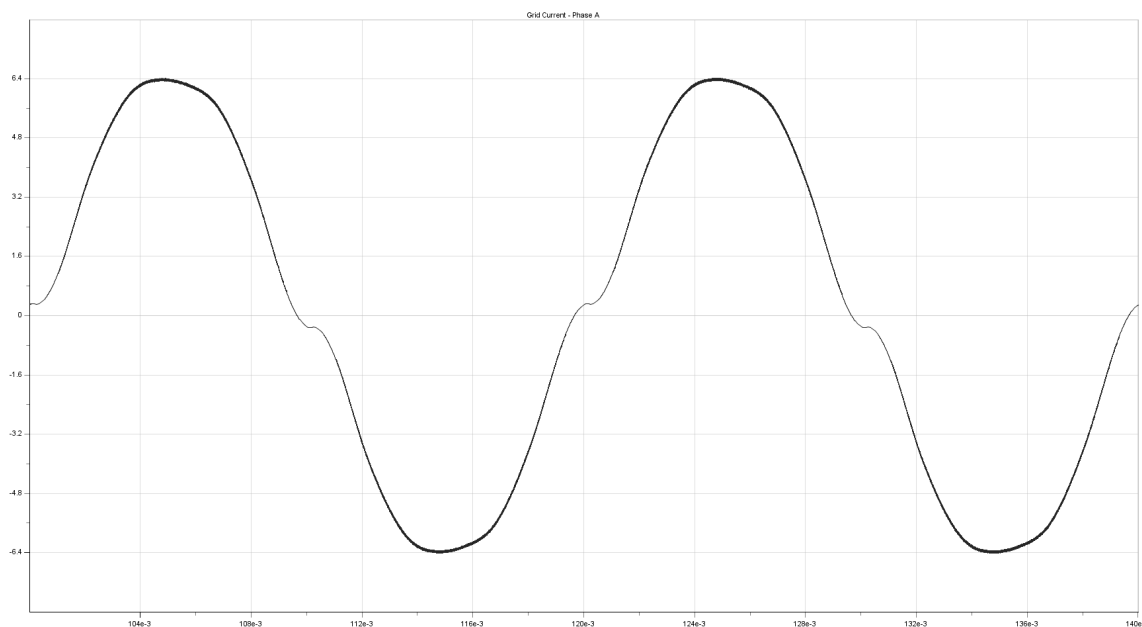


Figure 5.13: Effect of closed loop response on Three phase inductor current. X-axis depicts the time in seconds (sec) and Y-axis depicts the current in ampere (A).

6

Conclusion

The idea of charging electric vehicles through wireless power transfer is a continuously developing concept. This thesis dealt with the modelling and analysis of matrix converter for this application. In this thesis, the following research was conducted and workflow is highlighted below.

- Chapter 1 introduced the concept of WPT for EV charging, the use of matrix converter for the application and defined the motivation, problem statement and research questions for this thesis.
- Chapter 2 dealt with the understanding of wireless power transfer mechanism and the detailed background on the complete module for EV applications. A comparison on different available power supply topologies were tabulated.
- Chapter 3 gave an introduction to matrix converter. It also explained different switching configurations, commutation and the need for input filters.
- Chapter 4 dealt with the design of single phase matrix converter for the chosen WPT system. The feasibility of the designed converter was checked through simulations. The injection of harmonics into grid current due to the WPT system, was studied by comparing the results with the standards.
- Chapter 5 dealt with the design of three phase matrix converter. The feasibility of the power electronic module was verified. The system efficiency, effect of bifurcation and its mitigation was studied. Finally, control of the converter was established to ensure balanced sinusoidal grid current and constant output power.

This thesis answers the following research questions as discussed below:

1. What are the possible configurations of power converters for the implementation of WPT in EV charging? What is the chosen configuration for this application?

The possible configurations of power converters are single-stage, two-stage and three-stage. The chosen configuration for this application is a single-stage power converter, the matrix converter.

2. How is the chosen configuration implemented for a single-phase grid connection?

The configuration chosen to implement a single-phase grid connection was an Indirect Matrix Converter module. This converter configuration was modelled and analysed using LTSpice.

3. Can the single-phase implementation be extended to a three-phase system? If yes, how?

Yes, the single-phase implementation can be extended to a three-phase system. This can be realised by connecting three single-phase modules in star and the Indirect Matrix Converter to the primary of the transformer while the secondary of the transformer is connected in series to the resonant tank model.

6.1. Discussion

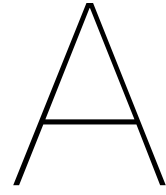
Establishing the research work done above, few inferences were made and are listed below.

- The literature review of WPT systems paved way in understanding the theory behind it. Use of conventional two stage converter leads to additional losses and components. Use of single stage converter would effectively transfer the desired power while ensuring reduced system losses.
- The configuration of power converter chosen: Rectifier + H-bridge based matrix converter, eased the design of gate drives which would have been arduous in case of 4-quadrant switches.
- The three phase system was made to operate in ZVS for all possible operating points of the load resistance. This was achieved by reducing the switching frequency of the converter to ensure the system operates in inductive region.

6.2. Future scope of work

This thesis provides a basic introduction to the implementation of matrix converter for WPT applications. However, further improvements can be made and few of the possible areas are recommended below.

- This thesis was validated only with the simulation results. Hardware implementation of the design helps in validating the system's feasibility.
- In the closed-loop control, the use of resonant controllers can be explored to attenuate harmonics other than the fundamental frequency to improve the grid-current waveforms.
- The effect of other compensation networks (Series-Parallel) on the matrix converter based WPT system can be explored.



Appendix

A.1. Fast Fourier Transform

Table A.1: Amplitude of currents obtained for different harmonic order with ideal LC filter for the inductor current from 4.21

Harmonic Number	Frequency [Hz]	Fourier Component
1	50	12.1355
2	100	118.2859e-6
3	150	221.214e-3
4	200	129.4977e-6
5	250	256.5662e-3
6	300	27.0773e-6
7	350	231.9237e-3
8	400	66.1097e-6
9	450	211.8493e-3
10	500	29.8345e-6
11	550	182.2667e-3
12	600	133.7091e-6
13	650	150.3316e-3
14	700	67.4014e-6
15	750	116.0064e-3
16	800	51.4534e-6
17	850	84.5176e-3
18	900	179.1968e-6
19	950	59.424e-3
20	1000	88.3877e-6
21	1050	42.4612e-3
22	1100	7.8051e-6
23	1150	35.6544e-3
24	1200	196.582e-6
25	1250	31.4903e-3
26	1300	120.425e-6
27	1350	29.0986e-3
28	1400	128.182e-6
29	1450	25.6103e-3
30	1500	302.7167e-6
31	1550	21.724e-3
32	1600	204.5064e-6
33	1650	20.2141e-3
34	1700	59.3969e-6
35	1750	17.5975e-3
36	1800	142.7361e-6
37	1850	15.8392e-3
38	1900	175.7712e-6
39	1950	15.0116e-3
40	2000	104.1465e-6

Table A.2: Amplitude of currents obtained for different harmonic order with damped LC filter for the inductor current from 4.22

Harmonic Number	Frequency [Hz]	Fourier Component
1	50	12.1351
2	100	102.8366e-6
3	150	221.1188e-3
4	200	98.2557e-6
5	250	256.5844e-3
6	300	56.4129e-6
7	350	231.9152e-3
8	400	104.0912e-6
9	450	211.7746e-3
10	500	22.524e-6
11	550	182.1317e-3
12	600	92.5585e-6
13	650	150.1412e-3
14	700	57.0485e-6
15	750	115.7962e-3
16	800	102.3748e-6
17	850	84.309e-3
18	900	121.1495e-6
19	950	59.2409e-3
20	1000	135.4844e-6
21	1050	42.2922e-3
22	1100	54.0988e-6
23	1150	35.4736e-3
24	1200	143.2106e-6
25	1250	31.2701e-3
26	1300	99.1736e-6
27	1350	28.8539e-3
28	1400	78.7361e-6
29	1450	25.3598e-3
30	1500	248.4158e-6
31	1550	21.5071e-3
32	1600	237.5217e-6
33	1650	20.0146e-3
34	1700	110.419e-6
35	1750	17.4367e-3
36	1800	95.5078e-6
37	1850	15.6797e-3
38	1900	145.244e-6
39	1950	14.836e-3
40	2000	119.9826e-6

Table A.3: Peak currents obtained for different harmonic component for the inductor current from 5.7

Harmonic Number	Frequency [Hz]	Fourier Component
1	50	5.6022
2	100	8.0836e-3
3	150	154.7445e-3
4	200	2.4105e-3
5	250	400.7943e-3
6	300	408.1764e-6
7	350	191.6944e-3
8	400	98.3053e-6
9	450	120.094e-3
10	500	42.9697e-6
11	550	37.7085e-3
12	600	56.1834e-6
13	650	21.4882e-3
14	700	35.7302e-6
15	750	19.5112e-3
16	800	24.2141e-6
17	850	12.512e-3
18	900	15.3573e-6
19	950	7.4153e-3
20	1000	7.7566e-6
21	1050	3.7797e-3
22	1100	19.3485e-6
23	1150	1.9303e-3
24	1200	30.7211e-6
25	1250	928.5161e-6
26	1300	26.3638e-6
27	1350	1.8907e-3
28	1400	22.8817e-6
29	1450	3.4131e-3
30	1500	25.5848e-6
31	1550	2.4719e-3
32	1600	34.6266e-6
33	1650	3.7095e-3
34	1700	10.5865e-6
35	1750	5.3613e-3
36	1800	21.4891e-6
37	1850	3.5706e-3
38	1900	23.4519e-6
39	1950	3.8629e-3
40	2000	41.7953e-6

Table A.4: Peak currents obtained for different harmonic order for the inductor current from 5.13

Harmonic Number	Frequency [Hz]	Fourier Component
1	50	6.3288
2	100	807.7579e-6
3	150	351.1814e-3
4	200	400.0237e-6
5	250	410.594e-3
6	300	80.82e-6
7	350	143.4727e-3
8	400	125.2396e-6
9	450	89.892e-3
10	500	114.1006e-6
11	550	37.1099e-3
12	600	202.0654e-6
13	650	5.3859e-3
14	700	58.7253e-6
15	750	8.9702e-3
16	800	41.0699e-6
17	850	8.2692e-3
18	900	88.2596e-6
19	950	8.2615e-3
20	1000	189.4741e-6
21	1050	5.4009e-3
22	1100	238.5783e-6
23	1150	2.5183e-3
24	1200	179.4374e-6
25	1250	2.0632e-3
26	1300	218.2211e-6
27	1350	2.7252e-3
28	1400	36.2752e-6
29	1450	2.867e-3
30	1500	213.1818e-6
31	1550	546.5895e-6
32	1600	103.7366e-6
33	1650	918.675e-6
34	1700	51.0905e-6
35	1750	608.0108e-6
36	1800	227.0112e-6
37	1850	996.6962e-6
38	1900	42.1396e-6
39	1950	971.2428e-6
40	2000	63.9208e-6

A.2. Semiconductor Behaviour

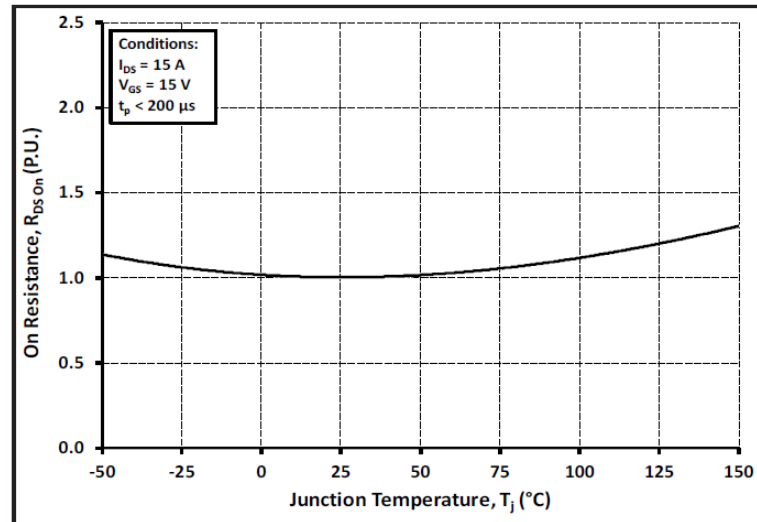


Figure A.1: MOSFET OnResistance Vs Temperature

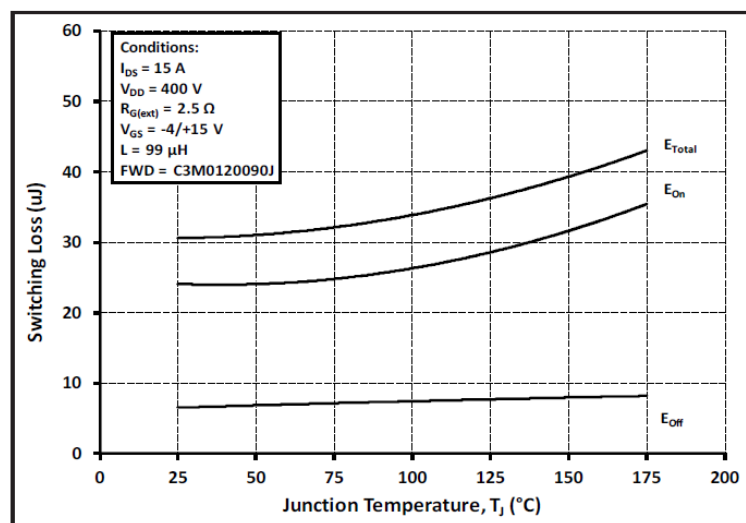


Figure A.2: MOSFET Switching Energy Vs Temperature

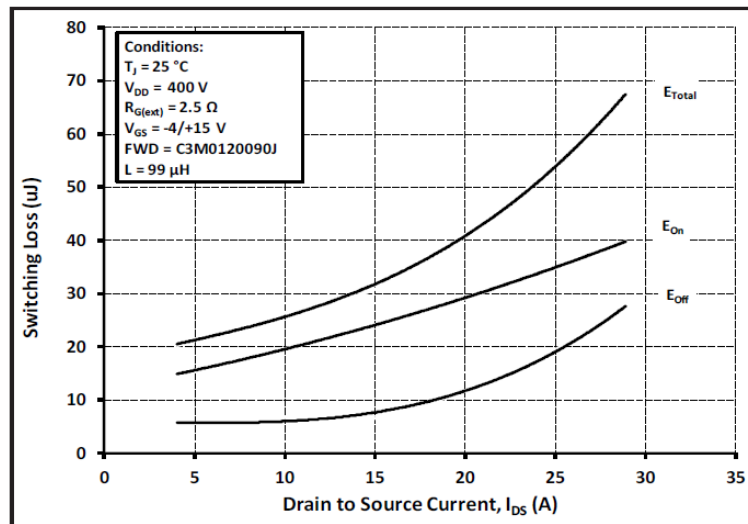


Figure A.3: MOSFET Switching Energy Vs Drain-Source Current

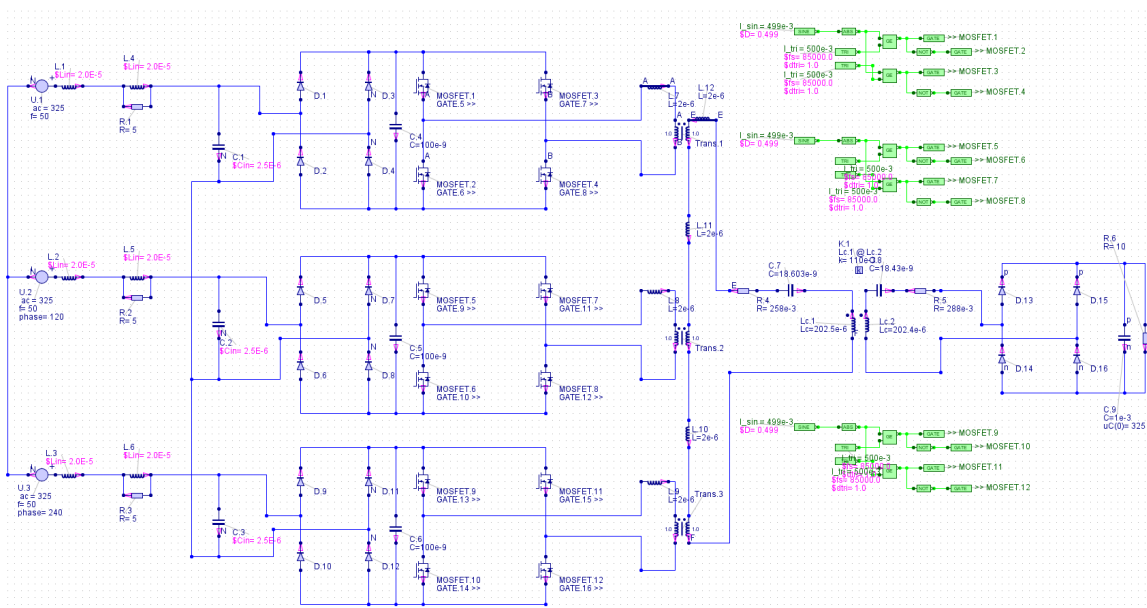


Figure A.4: Three-phase matrix converter DD coil-based WPT system.

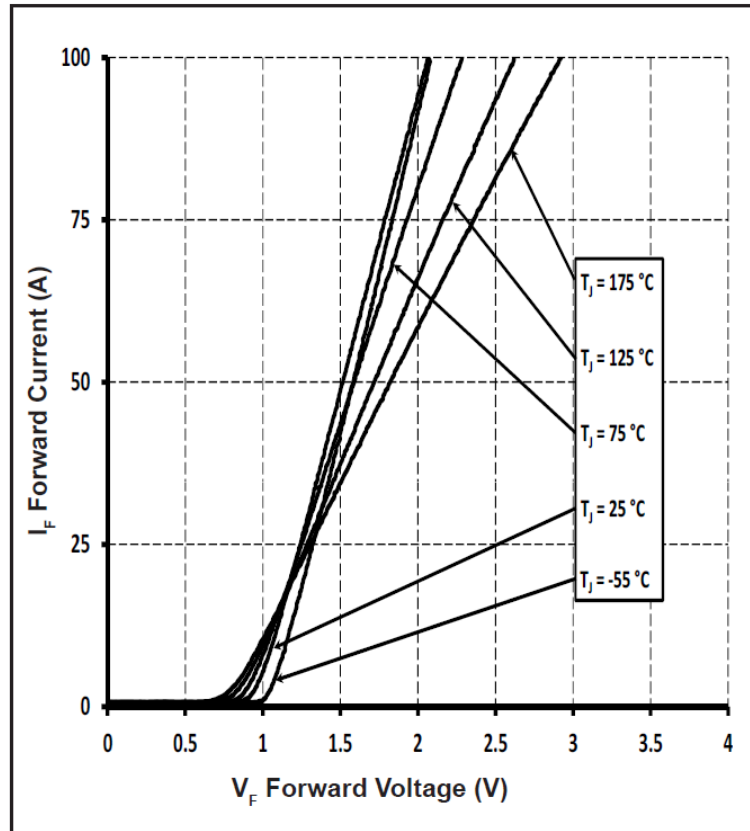


Figure A.5: Diode Forward Current Vs Forward Voltage

Bibliography

- [1] R. Zhao, D. T. Gladwin, and D. A. Stone. "Wireless power system applying a microcontroller dominated matrix converter". In: *IECON 2015 - 41st Annual Conference of the IEEE Industrial Electronics Society*. 2015, pp. 003405–003410. DOI: 10.1109/IECON.2015.7392626.
- [2] M. Venturini and A. Alesina. "The generalised transformer: A new bidirectional, sinusoidal waveform frequency converter with continuously adjustable input power factor". In: *1980 IEEE Power Electronics Specialists Conference*. 1980, pp. 242–252. DOI: 10.1109/PESC.1980.7089455.
- [3] H. Feng et al. "Advances in High-Power Wireless Charging Systems: Overview and Design Considerations". In: *IEEE Transactions on Transportation Electrification* 6.3 (2020), pp. 886–919. DOI: 10.1109/TTE.2020.3012543.
- [4] D. Patil et al. "Wireless Power Transfer for Vehicular Applications: Overview and Challenges". In: *IEEE Transactions on Transportation Electrification* 4.1 (2018), pp. 3–37. DOI: 10.1109/TTE.2017.2780627.
- [5] R. Bosshard, J. W. Kolar, and B. Wunsch. "Control method for Inductive Power Transfer with high partial-load efficiency and resonance tracking". In: *2014 International Power Electronics Conference (IPEC-Hiroshima 2014 - ECCE ASIA)*. 2014, pp. 2167–2174. DOI: 10.1109/IPEC.2014.6869889.
- [6] U. K. Madawala and D. J. Thrimawithana. "A Bidirectional Inductive Power Interface for Electric Vehicles in V2G Systems". In: *IEEE Transactions on Industrial Electronics* 58.10 (2011), pp. 4789–4796. DOI: 10.1109/TIE.2011.2114312.
- [7] S. Dieckerhoff, M. J. Ruan, and R. W. De Doncker. "Design of an IGBT-based LCL-resonant inverter for high-frequency induction heating". In: *Conference Record of the 1999 IEEE Industry Applications Conference. Thirty-Forth IAS Annual Meeting (Cat. No.99CH36370)*. Vol. 3. 1999, 2039–2045 vol.3. DOI: 10.1109/IAS.1999.806017.
- [8] S. Samanta and A. K. Rathore. "A new current-fed (C) (LC) (LC) topology for inductive wireless power transfer (IWPT) application: Analysis, design, and experimental results". In: *2015 IEEE Energy Conversion Congress and Exposition (ECCE)*. 2015, pp. 1279–1285. DOI: 10.1109/ECCE.2015.7309839.
- [9] H. R. Rahnamaee, U. K. Madawala, and D. J. Thrimawithana. "A multi-level converter for high power-high frequency IPT systems". In: *2014 IEEE 5th International Symposium on Power Electronics for Distributed Generation Systems (PEDG)*. 2014, pp. 1–6. DOI: 10.1109/PEDG.2014.6878623.
- [10] H. R. Rahnamaee, U. K. Madawala, and D. J. Thrimawithana. "A modified hybrid multi-level converter for high-power high-frequency IPT systems". In: *2014 International Power Electronics and Application Conference and Exposition*. 2014, pp. 624–629. DOI: 10.1109/PEAC.2014.7037929.
- [11] M. Bojarski et al. "Analysis and Control of Multiphase Inductively Coupled Resonant Converter for Wireless Electric Vehicle Charger Applications". In: *IEEE Transactions on Transportation Electrification* 3.2 (2017), pp. 312–320. DOI: 10.1109/TTE.2016.2566921.

- [12] M. Bojarski et al. "A 25 kW industrial prototype wireless electric vehicle charger". In: *2016 IEEE Applied Power Electronics Conference and Exposition (APEC)*. 2016, pp. 1756–1761. DOI: 10.1109/APEC.2016.7468105.
- [13] A. P. Hu, J. T. Boys, and G. A. Covic. "ZVS frequency analysis of a current-fed resonant converter". In: *7th IEEE International Power Electronics Congress. Technical Proceedings. CIEP 2000 (Cat. No.00TH8529)*. 2000, pp. 217–221. DOI: 10.1109/CIEP.2000.891417.
- [14] H. L. Li, A. P. Hu, and G. A. Covic. "A Direct AC–AC Converter for Inductive Power-Transfer Systems". In: *IEEE Transactions on Power Electronics* 27.2 (2012), pp. 661–668. DOI: 10.1109/TPEL.2011.2159397.
- [15] N. X. Bac, D. M. Vilathgamuwa, and U. K. Madawala. "A matrix converter based Inductive Power Transfer system". In: *2012 10th International Power Energy Conference (IPEC)*. 2012, pp. 509–514. DOI: 10.1109/ASSCC.2012.6523320.
- [16] D. J. Thrimawithana and U. K. Madawala. "A novel matrix converter based bi-directional IPT power interface for V2G applications". In: *2010 IEEE International Energy Conference*. 2010, pp. 495–500. DOI: 10.1109/ENERGYCON.2010.5771732.
- [17] D. S. B. Weerasinghe et al. "A three-phase to single-phase matrix converter based bi-directional IPT system for charging electric vehicles". In: *2013 IEEE ECCE Asia Doununder*. 2013, pp. 1240–1245. DOI: 10.1109/ECCE-Asia.2013.6579267.
- [18] J. Oyama et al. "New control strategy for matrix converter". In: *20th Annual IEEE Power Electronics Specialists Conference*. 1989, 360–367 vol.1. DOI: 10.1109/PESC.1989.48510.
- [19] V. C. JONES and B. K. BOSE. "A frequency step-up cycloconverter using power transistors in inverse-series mode". In: *International Journal of Electronics* 41.6 (1976), pp. 573–587. DOI: 10.1080/00207217608920668. eprint: <https://doi.org/10.1080/00207217608920668>. URL: <https://doi.org/10.1080/00207217608920668>.
- [20] L. Empringham, P. Wheeler, and J. Clare. "Intelligent commutation of matrix converter bi-directional switch cells using novel gate drive techniques". In: *PESC 98 Record. 29th Annual IEEE Power Electronics Specialists Conference (Cat. No.98CH36196)*. Vol. 1. 1998, 707–713 vol.1. DOI: 10.1109/PESC.1998.701976.
- [21] P. Wheeler, H. Zhang, and D. Grant. "A theoretical and practical consideration of optimised input filter design for a low loss matrix converter". In: *1994 Fifth International Conference on Power Electronics and Variable-Speed Drives*. 1994, pp. 363–367. DOI: 10.1049/cp:19940992.
- [22] P. Cortes et al. "New modulation and control scheme for phase-modular isolated matrix-type three-phase AC/DC converter". In: *IECON 2013 - 39th Annual Conference of the IEEE Industrial Electronics Society*. 2013, pp. 4899–4906. DOI: 10.1109/IECON.2013.6699928.
- [23] P. Cortes et al. "Detailed analysis and design of a three-phase phase-modular isolated matrix-type PFC rectifier". In: *2014 International Power Electronics Conference (IPEC-Hiroshima 2014 - ECCE ASIA)*. 2014, pp. 3864–3871. DOI: 10.1109/IPEC.2014.6870054.
- [24] L. Schrittwieser et al. "Modulation and Control of a Three-Phase Phase-Modular Isolated Matrix-Type PFC Rectifier". In: *IEEE Transactions on Power Electronics* 33.6 (2018), pp. 4703–4715. DOI: 10.1109/TPEL.2017.2726342.

- [25] *J2954: Wireless Power Transfer for Light-Duty Plug-in/Electric Vehicles and Alignment Methodology - SAE International*. URL: https://www-sae-org.tudelft.idm.oclc.org/standards/content/j2954_202010/ (visited on 07/27/2021).
- [26] F. Grazian et al. "Electric Vehicle Charging Based on Inductive Power Transfer Employing Variable Compensation Capacitance for Optimum Load Matching". In: *IECON 2020 The 46th Annual Conference of the IEEE Industrial Electronics Society*. 2020, pp. 5262–5267. DOI: 10.1109/IECON43393.2020.9254920.
- [27] F. Grazian et al. "Quality Factor Based Design Guideline for Optimized Inductive Power Transfer". In: *2020 IEEE PELS Workshop on Emerging Technologies: Wireless Power Transfer (WoW)*. 2020, pp. 178–183. DOI: 10.1109/WoW47795.2020.9291261.
- [28] T. Kume et al. "Integrated Filters and Their Combined Effects in Matrix Converter". In: *IEEE Transactions on Industry Applications* 43.2 (2007), pp. 571–581. DOI: 10.1109/TIA.2006.889971.
- [29] H. She et al. "Damped input filter design of matrix converter". In: *2009 International Conference on Power Electronics and Drive Systems (PEDS)*. 2009, pp. 672–677. DOI: 10.1109/PEDS.2009.5385684.
- [30] N. Mohan, T. M. Undeland, and W. P. Robbins. *Power Electronics: Converters, Applications, and Design*. 3rd ed. Hoboken, NJ: John Wiley & Sons, 2003. 802 pp. ISBN: 978-0-471-22693-2.
- [31] Z. Chen, D. Boroyevich, and J. Li. "Behavioral comparison of Si and SiC power MOSFETs for high-frequency applications". In: *2013 Twenty-Eighth Annual IEEE Applied Power Electronics Conference and Exposition (APEC)*. 2013, pp. 2453–2460. DOI: 10.1109/APEC.2013.6520640.
- [32] *Silicon Carbide Power MOSFET C3M™ MOSFET Technology*. C3M0120090J Rev. 2. CREE, Oct. 2020. URL: <https://www.wolfspeed.com/downloads/dl/file/id/834/product/646/c3m0120090j.pdf>.
- [33] *Silicon Carbide Schottky Diode*. C5D50065D Rev. A. CREE, Aug. 2016. URL: <https://cms.wolfspeed.com/app/uploads/2020/12/C5D50065D.pdf>.
- [34] Z. Qin. "Advanced Power Electronics (EE4515) - Lecture Slides". TU Delft (Delft).